mRNAs for the HHV-6 immediate-early and late genes in monocyte-derived DCs that had been inoculated with HHV-6B and cultured for 5 days (Fig. 1A). Quantitative real-time PCR analysis showed a large amount of HHV-6 copy in HHV-6B-inoculated monocyte-derived DCs 3 and 5 days after inoculation (Fig. 1B). In addition, flow cytometric analysis revealed the presence of HHV-6 antigen in these DCs (Fig. 1C). Moreover, infectious HHV-6 was recovered from them (data not shown). Similarly, replication of HHV-6A in monocyte-derived DCs was also detected (data not shown). These data demonstrate that both HHV-6A and HHV-6B can infect and replicate in monocyte-derived DCs. Because most of the HHV-6-infected monocyte-derived DCs were alive 5 days after inoculation, DCs harvested 5 days after HHV-6 inoculation were used in the following experiments.

Morphology of mock-infected and HHV-6-infected DCs

The morphologic differences between mock-infected and HHV-6-infected monocyte-derived DCs are shown in Figure 2. Inverted microscopy of mock-infected monocyte-derived DCs revealed the typical DC appearance with many dendritic processes; however, HHV-6-infected monocyte-derived DCs appeared to lack these processes and were instead round (Fig. 2A). These distinct morphologic differences were also detected by cytospin preparation with May-Giemsa staining (Fig. 2B) and transmission electron microscopy (Fig. 2C). Both DCs derived from mock-infected and HHV-6-infected monocytes were not adherent to plastic (data not shown).

Flow cytometric analysis of surface molecule expression on mock-infected and HHV-6-infected monocyte-derived DCs

We next examined alterations of surface molecule expression on HHV-6-infected monocyte-derived DCs. Upregulation of CD40, CD80, CD83, CD86, HLA class I, and HLA class II molecules was detected in HHV-6B-infected monocyte-derived immature DCs (Fig. 3). In contrast, expression level of CD209 (DC-SIGN) was decreased. On the other hand, surface molecule expression was not significantly different between mock-infected and HHV-6B-infected monocyte-derived mature DCs, except for CD209. Similar alterations of surface molecule expression were detected in HHV-6A-infected monocyte-derived DCs (data not shown). Inoculation of monocytes with ultraviolet-inactivated HHV-6 did not affect surface molecule expression on differentiated DCs (data not shown), suggesting that replication of HHV-6 is necessary to induce alterations in the expression of these molecules.

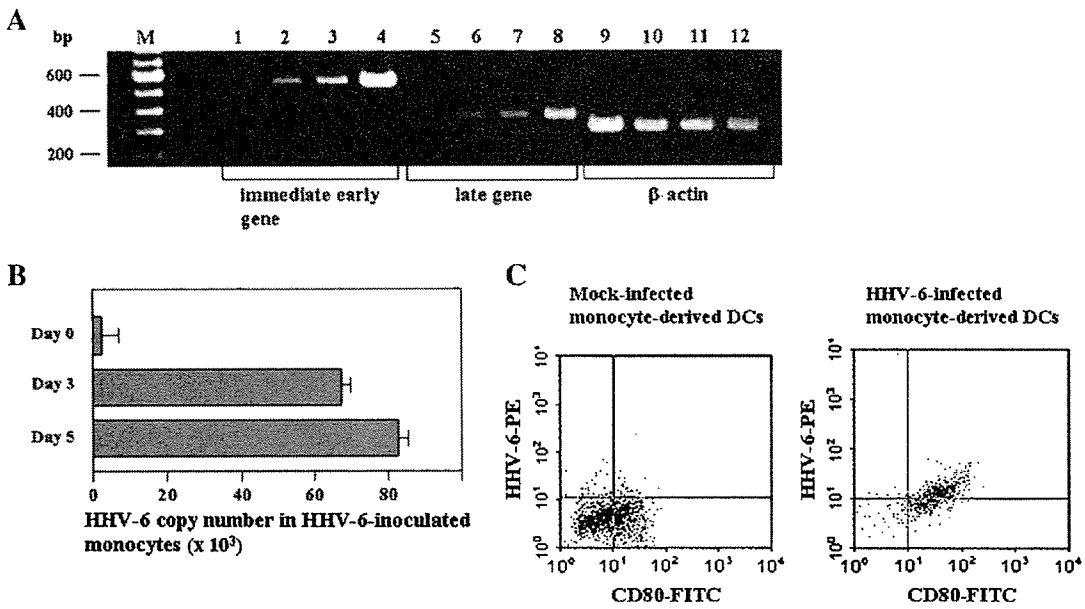

Figure 1. Replication of HHV-6 in monocyte-derived DCs. **(A):** Expression of HHV-6 mRNA in DCs. cDNAs synthesized from mock-infected monocyte-derived DCs (lanes 1, 5, and 9), HHV-6B-infected monocyte-derived DCs on day 3 after inoculation (lanes 2, 6, and 10), HHV-6B-infected monocyte-derived DCs on day 5 after inoculation (lanes 3, 7, and 11), and HHV-6B-infected cord blood mononuclear cells (lanes 4, 8, 12) were amplified using primers corresponding to the HHV-6 immediate-early and late genes and primers corresponding to the β-actin gene. Lane M shows marker DNAs. **(B):** Quantitative real-time PCR for the HHV-6 genome in monocyte-derived DCs. Mock-infected and HHV-6B-inoculated monocytes were cultured in the presence of GM-CSF and IL-4 for 3 or 5 days. DNAs were extracted from samples, and copy numbers of HHV-6 were estimated as described in Materials and Methods. **(C):** Flow cytometric analysis of HHV-6 antigen expression in monocyte-derived DCs. Mock-infected and HHV-6B-inoculated monocytes were cultured in the presence of GM-CSF and IL-4 for 5 days. Expression of cell surface CD80 and intracellular HHV-6 antigen was then examined by two-color flow cytometry.

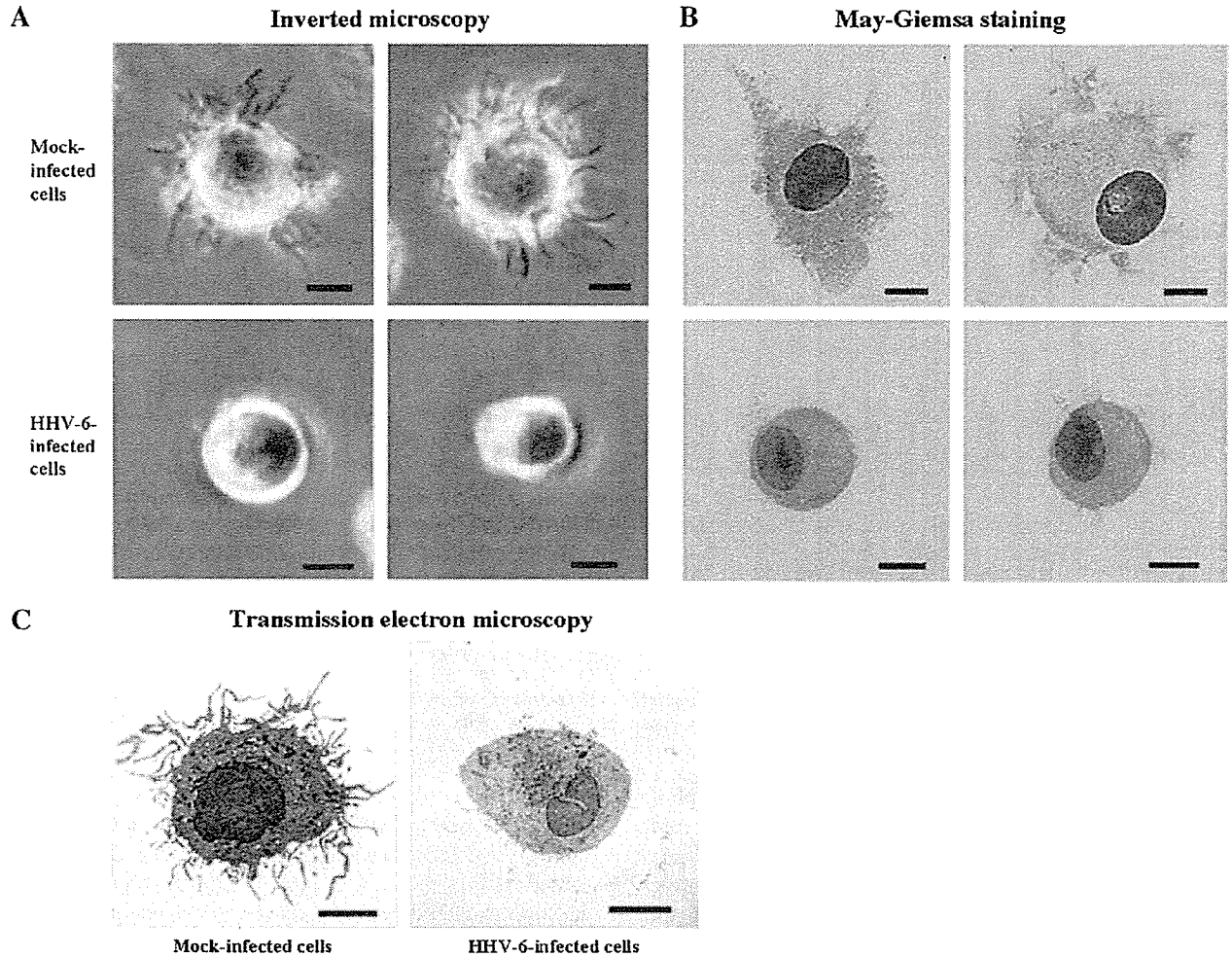

Figure 2. Morphologies of mock-infected and HHV-6-infected monocyte-derived DCs. Mock-infected and HHV-6B-inoculated monocytes were cultured in the presence of GM-CSF and IL-4 for 5 days. Morphologies of monocyte-derived DCs were examined by inverted microscopy **(A)**, after May-Giemsa staining of cytospin preparations **(B)**, and transmission electron microscopy (×1500) **(C)**. The bars represent 5 μm.

Reduced endocytosis by HHV-6-infected monocyte-derived DCs

Because uptake of antigens is an important function of DCs, we investigated whether HHV-6 infection affects the antigen-capture capacity of monocyte-derived DCs. Figure 4 shows the endocytosis profiles of mock-infected, HHV-6A-infected, and HHV-6B-infected monocyte-derived immature and mature DCs. The level of endocytosis mediated by HHV-6-infected monocyte-derived immature DCs was significantly lower than that mediated by mock-infected monocyte-derived immature DCs.

Reduced allostimulatory capacity of HHV-6-infected monocyte-derived DCs

The antigen-presentation capacity of mock-infected and HHV-6-infected monocyte-derived DCs was first examined by determining the stimulatory capacity of alloantigens. Allogeneic T lymphocytes isolated from donors whose HLA class I and class II types were nonidentical with those of the monocyte donors were cocultured with various numbers of monocyte-derived DCs. The allostimulatory capacity of HHV-6-infected monocyte-derived DCs was significantly lower than that of DCs derived from mock-infected monocytes (Fig. 5). The same experiments were performed three times and similar data were obtained (data not shown). These data indicate that HHV-6 infection alters the antigen-presentation capacity of monocytes.

Reduced viral antigen-stimulatory capacity of HHV-6-infected monocyte-derived DCs

We next examined the capacity of mock-infected and HHV-6-infected monocyte-derived DCs to present exogenous viral antigen. Exogenous antigens were at first captured, processed, and then presented to mainly antigen-specific $CD4^+$ T lymphocytes by the APCs, in the context of major histocompatibility complex class II molecules. Figure 6

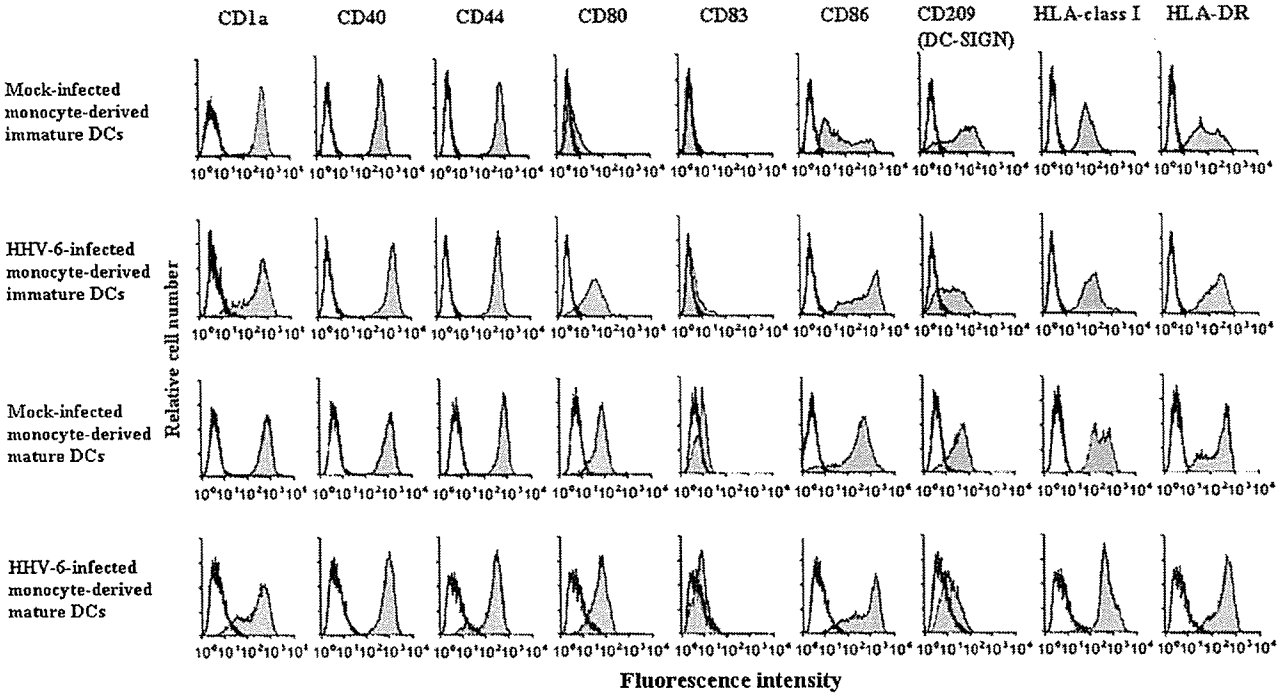

Figure 3. Flow cytometric analysis of mock-infected and HHV-6-infected monocyte-derived immature and mature DCs. Cell surface expression levels of CD1a, CD40, CD44, CD80, CD83, CD86, CD209 (DC-SIGN), HLA class I, and HLA-DR on the four types of DCs were measured by flow cytometry.

shows the proliferative responses of autologous T lymphocytes to HSV-1 antigen in the presence of mock-infected and HHV-6-infected monocyte-derived DCs. In the same manner as the response to alloantigens, the proliferative response of T lymphocytes to exogenous HSV-1 antigen was significantly lower when HHV-6A-infected or HHV-6B-infected monocyte-derived DCs were used as APCs than when DCs derived from mock-infected monocytes were used. The same experiments were performed three times, and similar data were obtained (data not shown). These data indicate that the pathway of presentation of exogenous antigens in monocyte-derived DCs is also impaired by HHV-6 infection.

Reduced peptide antigen-stimulatory capacity of HHV-6-infected monocyte-derived DCs

We examined further the presentation capacity of a 17-mer peptide that could be presented to peptide-specific $CD4^+$ T lymphocytes unnecessarily by being captured and processed by APCs. As we reported previously, the BCR-ABL fusion peptide-specific $CD4^+$ T-lymphocyte clone, MY-1, proliferates in response to stimulation with a BCR-ABL peptide in the presence of HLA-DRB1*0901-positive APCs. The proliferative response of MY-1 to the synthetic peptide in the presence of mock-infected or HHV-6-infected HLA class II–matched monocyte-derived DCs is shown in Figure 7. The degree of proliferative response mediated by MY-1 to the synthetic peptide appeared to be slightly lower when HHV-6-infected monocyte-derived DCs were used as APCs than when mock-infected monocyte-derived DCs were used. Taken together, the data presented in Figures 3, 4, 5, and 6 suggest strongly that in addition to alterations of antigen capture and antigen processing capacities, suppressor factor(s) may be produced by HHV-6-infected monocytes.

Production of suppressor factor(s) by HHV-6-infected monocytes

The data shown above suggest that the dysfunction of antigen presentation by HHV-6-infected monocyte-derived DCs is due to the production of immunosuppressive factor(s) in addition to the impairment of uptake and processing of antigens. We therefore verified that T-lymphocyte activation is suppressed by factor(s) produced from HHV-6-infected monocytes. Because IL-10 is a strongly immunosuppressive cytokine and is produced by monocytes, our investigation was focused on IL-10. The concentrations of IL-10 in the culture supernatants of mock-infected and HHV-6-infected monocytes were less than 20 pg/mL ($n = 4$) and 102 ± 10 pg/mL ($n = 4$), respectively. Adding culture supernatant of HHV-6-infected monocytes resulted in a reduced proliferative response of the BCR-ABL peptide-specific $CD4^+$ T-cell clone, MY-1, to stimulation with the peptide (Fig. 8). This inhibitory effect of the culture supernatant appeared to be partly inhibited by anti-IL-10 neutralizing antibody. These data indicate that

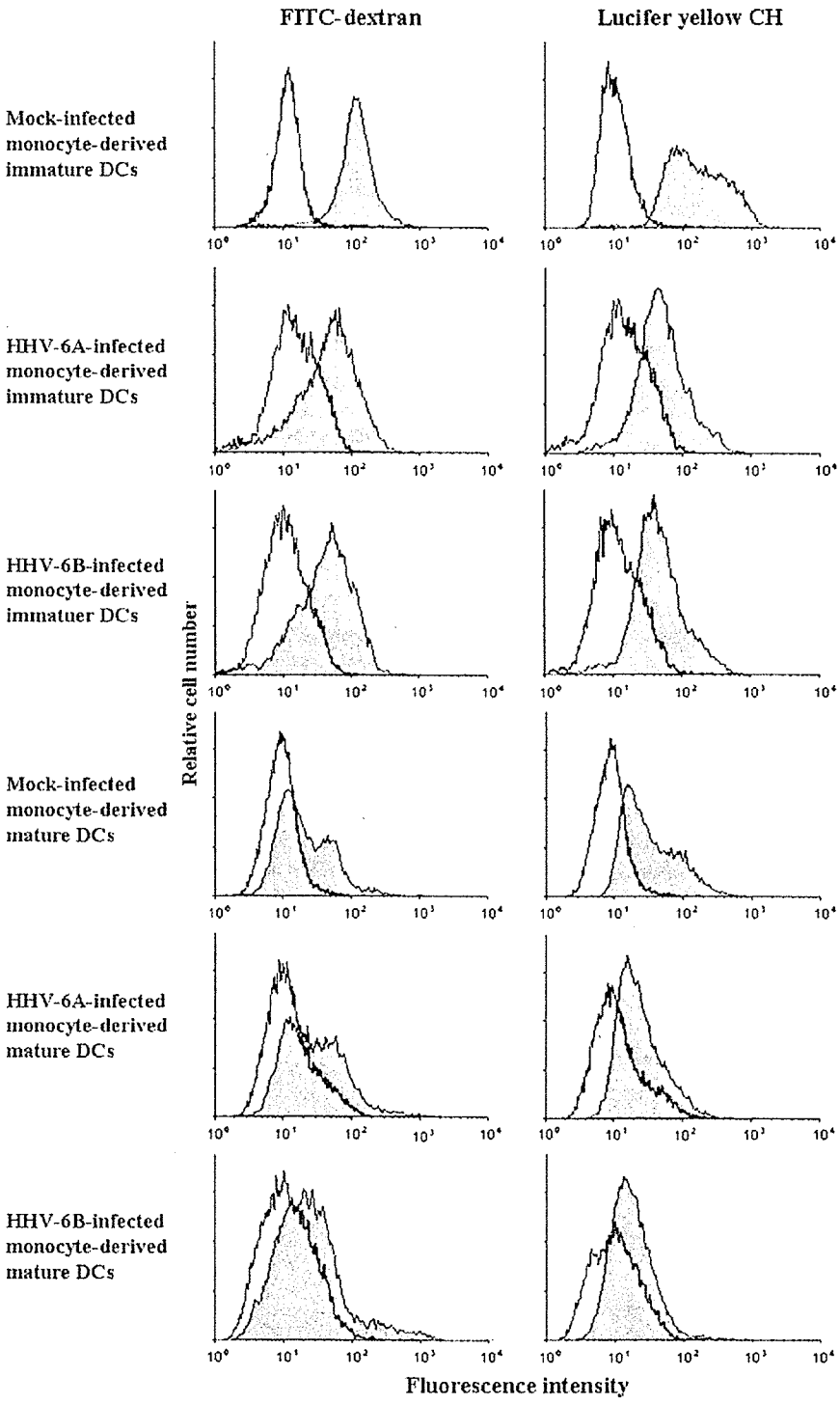

Figure 4. Flow cytometric analysis of endocytosis mediated by mock-infected, HHV-6A-infected, and HHV-6B-infected monocyte-derived immature and mature DCs. The six types of DCs were incubated in a medium containing FITC-dextran or Lucifer yellow CH at 37°C for 30 minutes (shaded histograms). The controls were evaluated by incubating cells in a medium containing FITC-dextran or Lucifer yellow CH at 4°C (clear histograms).

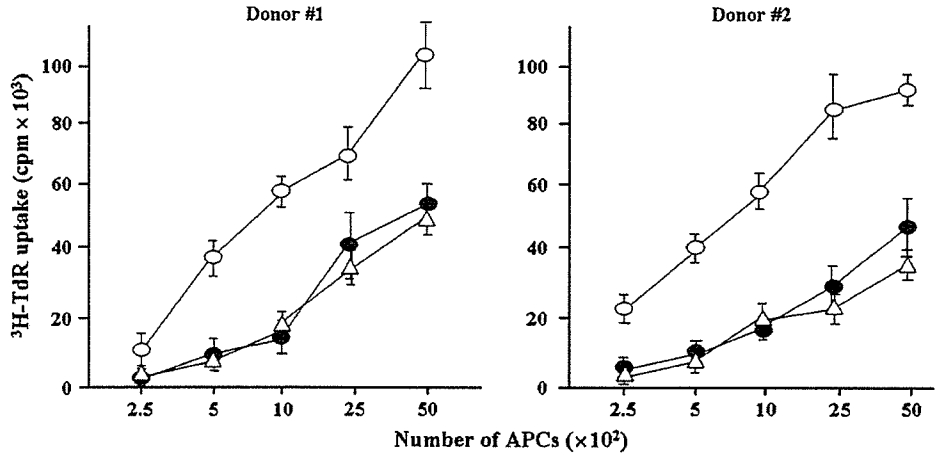

Figure 5. Presentation of alloantigens to allogeneic T lymphocytes by mock-infected and HHV-6-infected monocyte-derived DCs. Incorporation of [^{3}H]TdR into allogeneic T lymphocytes was determined in the presence of mock-infected monocyte-derived DCs (open circles), HHV-6A-infected monocyte-derived DCs (open triangles), or HHV-6B-infected monocyte-derived DCs (closed circles). Data represent means ± SDs of quadruplicate wells.

immunosuppressive factors, including IL-10, are produced by HHV-6-infected monocytes.

Impairment of antigen presentation by monocyte-derived DCs in a patient with HHV-6 reactivation

As mentioned above, HHV-6 infection of monocytes resulted in severe alteration of their antigen-presenting capacity in vitro. To confirm that this phenomenon also occurs in vivo, we examined the antigen-presenting capacity of monocyte-derived DCs isolated from a patient with DIHS who had severe HHV-6 viremia. Because the number of monocytes obtained from the patient was limited and the patient was negative for HLA-DR9, which is the restriction element of the peptide-specific T-cell clone MY-1, only the capacity to present alloantigen could be examined. Monocyte-derived DCs were generated from this patient during both HHV-6 viremia, when the number of copies of the HHV-6 genome in the PBMCs amounted to 11,000/μg DNA, and recovery, when the number of copies was 0/μg DNA. The allostimulatory capacity of monocyte-derived DCs isolated from the patient during HHV-6 viremia was significantly lower than that of mock-infected monocyte-derived DCs isolated from the patient in the recovery phase

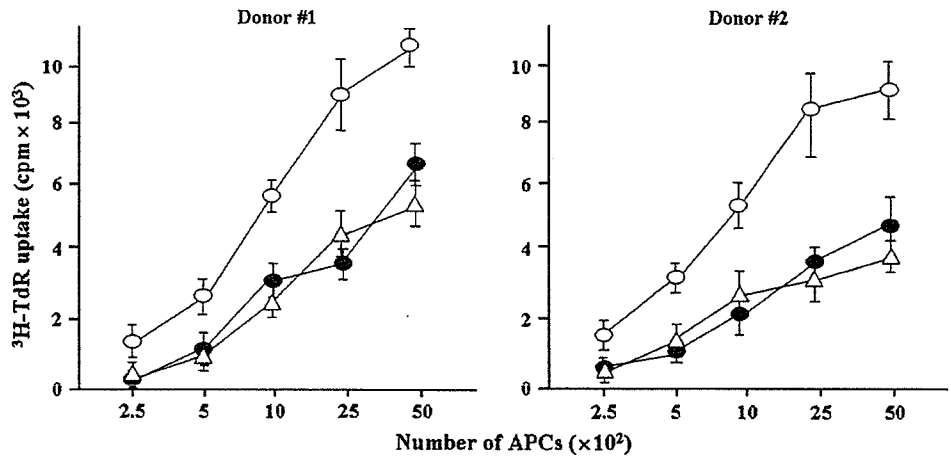

Figure 6. Presentation of exogenous HSV antigen to autologous T lymphocytes by mock-infected and HHV-6-infected monocyte-derived DCs. Incorporation of [^{3}H]TdR into autologous T lymphocytes was determined in the presence of mock-infected monocyte-derived DCs (open circles), HHV-6A-infected monocyte-derived DCs (open triangles), or HHV-6B-infected monocyte-derived DCs (closed circles) with or without viral antigen. The antigen-specific proliferative response of T lymphocytes was measured by subtracting the count obtained from preparations with no antigen stimulation from that obtained with HSV antigen stimulation. Data represent means ± SDs of quadruplicate wells.

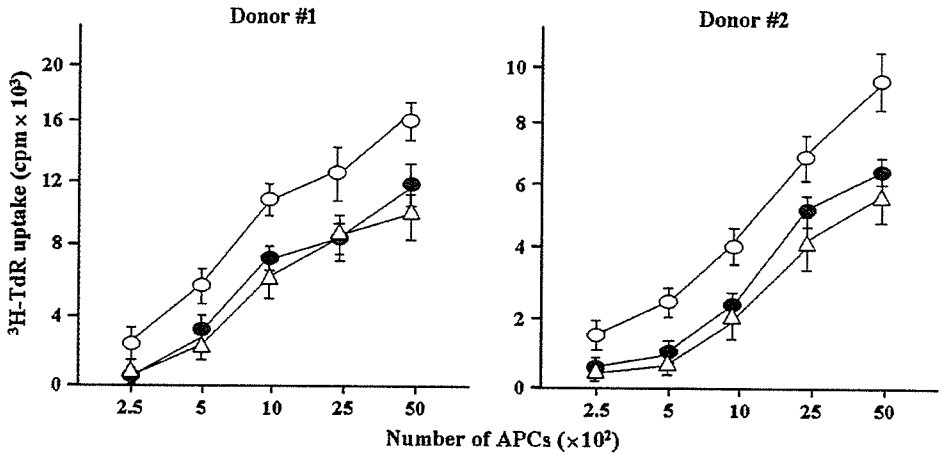

Figure 7. Presentation of peptide to a peptide-specific T-lymphocyte clone by mock-infected and HHV-6-infected monocyte-derived DCs. Incorporation of [^{3}H]TdR into BCR-ABL peptide-specific T-lymphocyte clones was determined in the presence of mock-infected monocyte-derived DCs (open circles), HHV-6A-infected monocyte-derived DCs (open triangles), or HHV-6B-infected monocyte-derived DCs (closed circles), with or without the BCR-ABL peptide at a concentration of 10 μM. Data represent means ± SDs of quadruplicate wells.

(Fig. 9). These data suggest strongly that impairment of antigen presentation by monocyte-derived DCs certainly occurs in vivo as well as in vitro.

Discussion

Because the induction of altered DC function by viral infection is an important issue in the pathogenesis of virus-induced immunodeficiency, studies focusing on the effects of viral infection on the phenotype and function of DCs have been reported. Various viruses affect the maturation of DCs. For example, vaccinia virus inhibits DC maturation, thus reducing the capacity of DCs to stimulate T lymphocytes [36]. A similar phenomenon has also been demonstrated in HSV-infected DCs [37]. Although some

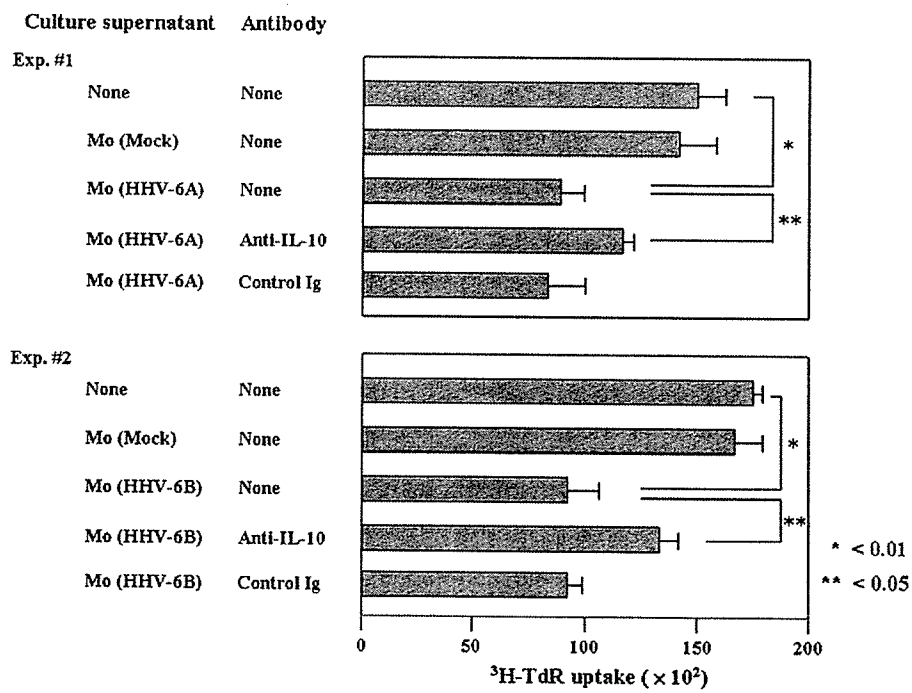

Figure 8. Effects of culture supernatants of mock-infected and HHV-6-infected monocytes on proliferative response of T-lymphocyte clone. Culture supernatants of mock-infected and HHV-6-infected monocytes were collected 3 days after infection. The proliferative response of BCR-ABL-specific T-lymphocyte clone to stimulation with BCR-ABL peptide in the presence or absence of culture supernatant was examined as described above. In some experiments, the culture supernatants were incubated with anti-IL-10 neutralizing antibody before being added to the culture wells. Data represent means ± SDs of quadruplicate wells.

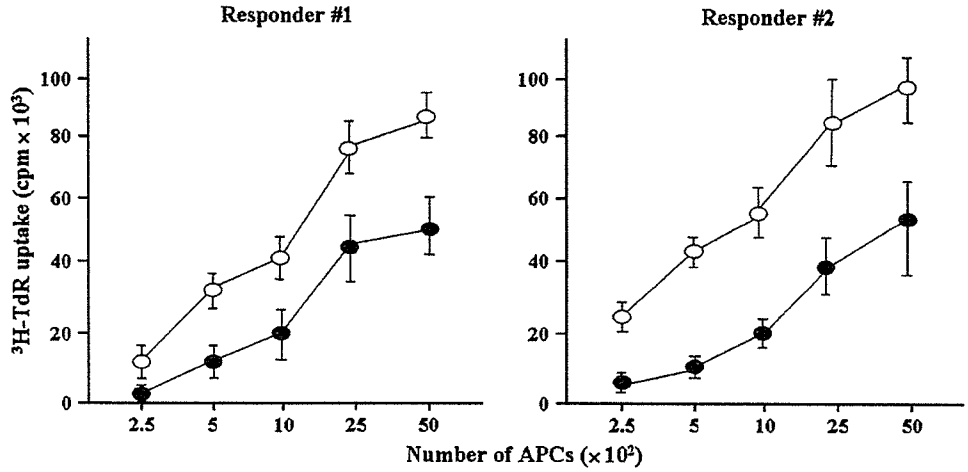

Figure 9. Presentation of alloantigens to allogeneic T lymphocytes by monocyte-derived DCs from a patient with DIHS. Monocyte-derived DCs were generated from PBMCs of the DIHS patient during the HHV-6 viremia and recovery phases. Incorporation of [^{3}H]TdR into allogeneic T lymphocytes was determined in the presence of monocyte-derived DCs generated during HHV-6 viremia (closed circles) or the recovery phase (open circles). Data represent means ± SDs of quadruplicate wells.

viruses impair the process of maturation of DCs, other viruses have been shown to drive DC maturation. Measles virus infection of immature DCs induces DC maturation and dysfunction of their capacity to stimulate T lymphocytes [38–40]. It has also been reported that dengue virus infection of immature DCs leads to their maturation [41]. We reported recently that HHV-6 infection of immature DCs results in impairment of antigen-presentation capacity, despite phenotypic maturation [24].

Because monocytes are the major source of myeloid DCs and HHV-6 latently infects monocytes, we investigated the morphologic and functional effects of HHV-6 infection on the differentiation of monocytes to DCs. Consequently, we found the following evidence. First, the morphology of DCs differentiated from HHV-6-infected monocytes is distinctly different from that of DCs differentiated from mock-infected monocytes. Second, the levels of expression of DC-associated molecules, such as CD80, CD83, and CD86, are higher on HHV-6-infected monocyte-derived DCs than on mock-infected monocyte-derived DCs. Third, the antigen-uptake capacity of HHV-6-infected monocyte-derived DCs is lower than that of DCs derived from mock-infected monocytes. Fourth, the capacity to present antigens such as alloantigen, exogenous viral antigen, and epitope peptide is lower in HHV-6-infected monocyte-derived DCs than in mock-infected monocyte-derived DCs, and DCs derived from HHV-6-infected monocytes produce immunosuppressive factors, including IL-10. Finally, DCs generated from monocytes isolated from a patient with severe HHV-6 reactivation showed impairment of antigen-presentation capacity, suggesting strongly that HHV-6-induced dysfunction of monocyte-derived DCs occurs in patients with HHV-6 infection.

An interesting finding of our study is the morphology of HHV-6-infected monocyte-derived DCs. Although mock-infected monocytes had the typical DC appearance after incubation with GM-CSF and IL-4, as described previously [29], DCs derived from HHV-6-infected monocytes were round and lacked dendritic processes. It has been reported that syncytium formation of DCs is induced by measles virus infection [38–40]; however, the morphologic changes induced in DCs by infection with other viruses have not been precisely reported. Although the mechanism of alteration of the morphology of HHV-6-infected monocyte-derived DCs is unknown, active replication of HHV-6 may be required to induce such changes, because DCs derived from monocytes inoculated with inactivated HHV-6 showed the typical DC appearance (data not shown).

Our most important finding is that antigen-presenting capacity, which is the professional function of DCs, is severely impaired in HHV-6-infected monocyte-derived DCs. Impairment of the antigen-presenting capacity of DCs has been reported in various viral infections. In most studies reported previously, only the alloantigen-stimulatory capacity of DCs to allogeneic T lymphocytes has been used to evaluate antigen-presenting capacity. We performed a precise examination of the antigen-presenting capacity of DCs using exogenous viral antigen and a peptide antigen unnecessarily captured and processed by DCs. Moreover, we also examined the capacity of DCs for antigen capture by flow cytometric analysis of endocytosis. Consequently, we found that the antigen-presenting capacity of HHV-6-infected monocyte-derived DCs is impaired in several ways. First, antigen-capture capacity is decreased. Second, processing of endogenous and exogenous antigens may also be impaired. Third, the capacity to present peptide that can

bind to HLA molecules unnecessarily by being captured and processed by DCs is also decreased, despite normal expression of HLA and costimulatory molecules, suggesting strongly that immunosuppressive factor(s) may be produced by HHV-6-infected monocyte-derived DCs.

Because IL-10 is one of the major immunosuppressive cytokines and is known to be produced by virus-infected DCs, we further studied the mechanisms of DC dysfunction induced by HHV-6 infection, focusing on IL-10. Production of IL-10 was detected in the culture supernatant of HHV-6-infected monocytes as described previously [42], and adding anti-IL-10 antibody resulted in partial reduction of the inhibitory effect of culture supernatant of HHV-6-infected monocytes on the proliferative response of T lymphocytes. These data indicate that production of IL-10 is one of the causes of the monocyte-derived DC dysfunction induced by HHV-6 infection. Li and colleagues reported that HHV-6 infection induced the production of IL-10 and IL-12 by monocytes. Expression of IL-12 mRNA decreased with accumulation of IL-10 mRNA, and production of IL-12 was increased when anti-IL-10 mAb was added to the cultures, implying that endogenous IL-10 induced by HHV-6 infection inhibited IL-12 production [43]. Selective suppression of IL-12 production induced by HHV-6 infection independently of viral replication was also reported [44,45]. Disharmony of cytokine production—that is, overproduction of IL-10 and suppression of IL-12—may result in impairment of the protective immune response against HHV-6. Interestingly, the relationship between IL-10 production by monocytes and dysfunction of monocyte-derived DCs has also been speculated upon in regard to human cytomegalovirus [46], which is a β-herpesvirus similar to HHV-6, suggesting that there are common mechanisms of IL-10 production by DCs in β-herpesvirus infections.

The various effects of HHV-6 on cellular functions have been clarified. However, these data were obtained from in vitro experimental systems; therefore, it is doubtful whether the same phenomena occur in vivo. Because HHV-6 infection is restricted to humans, no animal model is available. HHV-6 reactivation occurs frequently in patients with immunodeficiency diseases or conditions, such as hematopoietic stem cell transplantation, organ transplantation, and AIDS. However, the functions of monocytes and DCs are also affected by underlying diseases and immunosuppressive drugs; therefore, monocytes obtained from these immunodeficient patients do not seem suitable for examining the effect of HHV-6 infection in vivo. To overcome these problems, we used monocytes isolated from a patient with DIHS. The pathogenesis of this condition has recently been clarified. In patients with DIHS, severe HHV-6 reactivation is induced following drug allergy [47]. Because DIHS occurs in immunocompetent patients, the monocytes and lymphocytes of these patients seem to be useful for studying the biologic effects of HHV-6 infection on the immune system in vivo. Our data clearly showed that HHV-6-induced impairment of DC differentiation from monocytes certainly occurs in vivo.

In summary, we found that differentiation of myeloid DCs from monocytes is severely impaired by infection with either HHV-6A or HHV-6B. Our present data suggest a novel concept for the mechanism of HHV-6-induced immunodeficiency. In light of the evidence that HHV-6 reactivation occurs frequently in immunodeficient patients, clarification of the pathogenesis of HHV-6-induced immunodeficiency and restoration of the impaired immune system in HHV-6 infection seem important issues.

Acknowledgment

We are grateful for the skilled technical assistance of Ms. Yuka Sato. This work was supported by grants from the Ministry of Education, Culture, Sports, Science and Technology of Japan, and the Ministry of Health, Labor and Welfare of Japan.

References

1. Yoshikawa T. Human herpesvirus 6 infection in hematopoietic stem cell transplant patients. Br J Haematol. 2004;124:421–432.
2. Lusso P, Gallo RC. Human herpesvirus 6 in AIDS. Immunol Today. 1995;16:67–71.
3. Akashi K, Eizuru Y, Sumiyoshi Y, et al. Severe infectious mononucleosis-like syndrome and primary human herpesvirus 6 infection in an adult. N Engl J Med. 1993;329:168–171.
4. Sugita K, Kurumada H, Eguchi M, Furukawa T. Human herpesvirus 6 infection associated with hemophagocytic syndrome. Acta Haematol. 1995;93:108–109.
5. Tohyama M, Yahata Y, Yasukawa M, et al. Severe hypersensitivity syndrome due to sulfasalazine associated with reactivation of human herpesvirus 6. Arch Dermatol. 1998;134:1113–1117.
6. Yamanishi K. Human herpesvirus 6. Microbiol Immunol. 1992;36: 551–561.
7. Braun DK, Dominguez G, Pellett PE. Human herpesvirus 6. Clin Microbiol Rev. 1997;10:521–562.
8. De Bolle L, Naesens L, De Clercq E. Update on human herpesvirus 6 biology, clinical features, and therapy. Clin Microbiol Rev. 2005;18: 217–245.
9. Salahuddin SZ, Ablashi DV, Markham PD, et al. Isolation of a new virus, HBLV, in patients with lymphoproliferative disorders. Science. 1986;234:596–601.
10. Ablashi DV, Lusso P, Hung CL, et al. Utilization of human hematopoietic cell lines for the propagation and characterization of HBLV (human herpesvirus 6). Int J Cancer. 1988;42:787–791.
11. Luka J, Okano M, Thiele G. Isolation of human herpesvirus-6 from clinical specimens using human fibroblast cultures. J Clin Lab Anal.1990;4:483–486.
12. He J, McCarthy M, Zhou Y, Chandran B, Wood C. Infection of primary human astrocytes by human herpesvirus 6. J Virol. 1996;70: 1296–1300.
13. Inagi R, Guntapong R, Nakao M, et al. Human herpesvirus 6 induces IL-8 gene expression in human hepatoma cell line, Hep G2. J Med Virol. 1996;49:34–40.
14. Isomura H, Yamada M, Yoshida M, et al. Suppressive effects of human herpesvirus 6 on in vitro colony formation of hematopoietic progenitor cells. J Med Virol. 1997;52:406–412.
15. Yasukawa M, Ohminami H, Sada E, et al. Latent infection and reactivation of human herpesvirus 6 in two novel myeloid cell lines. Blood. 1999;93:991–999.
16. Lusso P, Malnati M, De Maria A, et al. Productive infection of $CD4^+$ and $CD8^+$ mature human T cell populations and clones by human

herpesvirus 6. Transcriptional down-regulation of CD3. J Immunol. 1991;147:685–691.
17. Furukawa M, Yasukawa M, Yakushijin Y, Fujita S. Distinct effects of human herpesvirus 6 and human herpesvirus 7 on surface molecule expression and function of $CD4^+$ T cells. J Immunol. 1994;152:5768–5775.
18. Lusso P, De Maria A, Malnati M, et al. Induction of CD4 and susceptibility to HIV-1 infection in human $CD8^+$ T lymhocytes by human herpesvirus 6. Nature. 1991;349:533–535.
19. Lusso P, Malnati MS, Garzino-Demo A, Crowley RW, Long EO, Gallo RC. Infection of natural killer cells by human herpesvirus 6. Nature. 1993;362:458–462.
20. Lusso P, Garzino-Demo A, Crowley RW, Malnati MS. Infection of γ/δ T lymphocytes by human herpesvirus 6: trascriptional induction of CD4 and susceptibility to HIV infection. J Exp Med. 1995;181: 1303–1310.
21. Horvat RT, Parmely MJ, Chandran B. Human herpesvirus 6 inhibits the proliferative responses of human peripheral blood mononuclear cells. J Infect Dis. 1993;167:1274–1280.
22. Yasukawa M, Hasegawa A, Sakai I, et al. Down-regulation of CXCR4 by human herpesvirus 6 (HHV-6) and HHV-7. J Immunol. 1999;162: 5417–5422.
23. Hasegawa A, Yasukawa M, Sakai I, Fujita S. Transcriptional down-regulation of CXCR4 induced by impaired association of transcription regulator YY1 with c-Myc in human herpesvirus 6-infected cells. J Immunol. 2001;166:1125–1131.
24. Kakimoto M, Hasegawa A, Fujita S, Yasukawa M. Phenotypic and functional alterations of dendritic cells induced by human herpesvirus 6 infection. J Virol. 2002;76:10338–10345.
25. Banchereau J, Briere F, Caux C, et al. Immunobiology of dendritic cells. Annu Rev Immunol. 2000;18:767–811.
26. Dauer M, Obermaier B, Herten J, et al. Mature dendritic cells derived from human monocytes within 48 hours: a novel strategy for dendritic cell differentiation from blood precursors. J Immunol. 2003;170: 4069–4076.
27. Chapuis F, Rosenzwajg M, Yagello M, Ekman M, Biberfeld P, Gluckman JC. Differentiation of human dendritic cells from monocytes in vitro. Eur J Immunol. 1997;27:431–441.
28. Zhou LJ, Tedder TF. $CD14^+$ blood monocytes can differentiate into functionally mature $CD83^+$ dendritic cells. Proc Natl Acad Sci U S A. 1996;93:2588–2592.
29. Kondo K, Kondo T, Okuno T, Takahashi M, Yamanishi K. Latent human herpesvirus 6 infection of human monocytes/macrophages. J Gen Virol. 1991;72:1401–1408.
30. Romani N, Reider D, Heuer M, et al. Generation of mature dendritic cells from human blood. An improved method with special regard to clinical applicability. J Immunol Methods. 1996;196:137–151.
31. Zou P, Isegawa Y, Nakano K, Haque M, Horiguchi Y, Yamanishi K. Human herpesvirus 6 open reading frame U83 encodes a functional chemokine. J Virol. 1999;73:5926–5933.
32. Ihira M, Yoshikawa T, Suzuki K, et al. Monitoring of active HHV-6 infection in bone marrow transplant recipients by real time PCR; comparison to detection of viral DNA in plasma by qualitative PCR. Microbiol Immunol. 2002;46:701–705.
33. Sallusto F, Cella M, Danieli C, Lanzavecchia A. Dendritic cells use macropinocytosis and the mannose receptor to concentrate macromolecules in the major histocompatibility complex class II compartment: downregulation by cytokines and bacterial products. J Exp Med. 1995; 182:389–400.
34. Yasukawa M, Inatsuki A, Horiuchi T, Kobayashi Y. Functional heterogeneity among herpes simplex virus-specific $CD4^+$ T cells. J Immunol. 1991;146:1341–1347.
35. Yasukawa M, Ohminami H, Kaneko S, et al. $CD4^+$ cytotoxic T-cell clones specific for bcr-abl b3a2 fusion peptide augment colony formation by chronic myelogenous leukemia cells in a b3a2-specific and HLA-DR-restricted manner. Blood. 1998;92:3355–3361.
36. Engelmayer J, Larsson M, Subklewe M, et al. Vaccinia virus inhibits the maturation of human dendritic cells: a novel mechanism of immune evasion. J Immunol. 1999;163:6762–6768.
37. Salio M, Cella M, Suter M, Lanzavecchia A. Inhibition of dendritic cell maturation by herpes simplex virus. Eur J Immunol. 1999;29: 3245–3253.
38. Fugier-Vivier I, Servet-Delprat C, Rivailler P, Rissoan MC, Liu YJ, Rabourdin-Combe C. Measles virus suppresses cell-mediated immunity by interfering with the survival and functions of dendritic and T cells. J Exp Med. 1997;186:813–823.
39. Grosjean I, Caux C, Bella C, et al. Measles virus infects human dendritic cells and blocks their allostimulatory properties for $CD4^+$ T cells. J Exp Med. 1997;186:801–812.
40. Schnorr JJ, Xanthakos S, Keikavoussi P, Kämpgen E, ter Meulen V, Schneider-Schaulies S. Induction of maturation of human blood dendritic cell precursors by measles virus is associated with immunosuppression. Proc Natl Acad Sci U S A. 1997;94:5326–5331.
41. Ho LJ, Wang JJ, Shaio MF, et al. Infection of human dendritic cells by dengue virus causes cell maturation and cytokine production. J Immunol. 2001;166:1499–1506.
42. Arena A, Stassi G, Speranza A, Iannello D, Mastroeni P. Modulatory effect of HHV-6 on MCP-1 production by human monocytes. New Microbiol. 2002;25:335–340.
43. Li C, Goodrich JM, Yang X. Interferon-gamma (IFN-gamma) regulates production of IL-10 and IL-12 in human herpesvirus-6 (HHV-6)-infected monocyte/macrophage lineage. Clin Exp Immunol. 1997;109:421–425.
44. Smith A, Santoro F, Di Lullo G, Dagna L, Verani A, Lusso P. Selective suppression of IL-12 production by human herpesvirus 6. Blood. 2003;102:2877–2884.
45. Smith A, Paolucci C, Di Lullo G, Burastero S, Santoro F, Lusso P. Viral replication-independent blockade of dendritic cell maturation and IL-12 production by human herpesvirus 6. J Virol. 2005;79:2807–2813.
46. Nordoy I, Rollag H, Lien E, et al. Cytomegalovirus infection induces production of human interleukin-10 in macrophages. Eur J Clin Microbiol Infect Dis. 2003;22:737–741.
47. Hashimoto K, Yasukawa M, Tohyama M. Human herpesvirus 6 and drug allergy. Curr Opin Allergy Clin Immunol. 2003;3:255–260.

Cell Tissue Res (2006) 326: 69–77
DOI 10.1007/s00441-006-0208-2

REGULAR ARTICLE

Lujun Yang · Yuji Shirakata · Masachika Shudou · Xiuju Dai · Sho Tokumaru · Satoshi Hirakawa · Koji Sayama · Junji Hamuro · Koji Hashimoto

New skin-equivalent model from de-epithelialized amnion membrane

Received: 14 December 2005 / Accepted: 23 March 2006 / Published online: 7 June 2006

Abstract The presence of pre-existing basement membrane (BM) components improves the morphogenesis of epidermis and BM in constructing a human living skin-equivalent (LSE). De-epithelialized amniotic membrane (AM) retains key BM components. We have therefore investigated the usefulness of AM for constructing LSE. De-epithelialized AM was overlaid on type I collagen gel embedded with fibroblasts. Normal human keratinocytes (NHKs) were then seeded onto the epithelial side of the AM to construct an AM-LSE. A conventional LSE was constructed by seeding NHKs on a fibroblast-populated type I collagen gel. When the keratinocytes reached confluence, the LSE was lifted to the air-liquid interface and cultured for up to 3 weeks. Samples were harvested at various times and investigated morphologically, immunohistochemically, and ultrastructurally. In AM-LSE, the epidermis was better stratified, with more compact, polarized, columnar basal cells, and the expression of differentiation and proliferation markers was more similar to that of normal human skin than was that of LSE without AM. A more continuous BM and better-developed hemidesmosomes were found in AM-LSE. The epidermis of AM-LSE outgrew much faster than that of LSE without AM. When transplanted onto nude mice, both LSEs took well; however, the AM-LSE graft showed better morphogenesis of the epidermis, BM, and hemidesmosomes. The better epidermal morphology and better-developed BM in AM-LSE in vitro and in vivo indicates its superiority over LSE without AM for clinical applications.

Keywords Amniotic membrane · Basement membrane · Keratinocyte · Migration · Skin-equivalent · Human · Mouse (BALB/cAJcl-nu)

This work was partly supported by Health Sciences Research Grants for Research on Specific Diseases from the Ministry of Health, Labor, and Welfare of Japan (to K.H.) and a Grant-in-Aid for Scientific Research from the Ministry of Education, Culture, Sports, Science, and Technology of Japan (to K.H. and Y.S.).
L. Yang and Y. Shirakata contributed equally to this work.

L. Yang · Y. Shirakata (✉) · X. Dai · S. Tokumaru · S. Hirakawa · K. Sayama · K. Hashimoto
Department of Dermatology,
Ehime University School of Medicine,
Shitsukawa,
Toon, Ehime 791-0295, Japan
e-mail: shirakat@m.ehime-u.ac.jp
Tel.: +81-89-9605350
Fax: +81-89-9605352

M. Shudou
Department of Bioscience, Ehime University,
Shitsukawa,
Toon, Ehime 791-0295, Japan

J. Hamuro
ArBlast,
Chuo-ku, Kobe 650-0047, Japan

Introduction

Living skin-equivalent (LSE), which consists of epidermis and dermis matrix, has long been used as a skin substitute for wound closure (Eaglstein and Falanga 1998). A well-developed differentiated epidermis provides a barrier against bacteria and other environmental factors, and the presence of a basement membrane (BM) and fibroblasts are necessary for maintaining epidermal architecture and sustaining growth (Andriani et al. 2003). A variety of biomaterials has been used to construct the dermal matrix of LSE (Guerret et al. 2003; Llames et al. 2004; Meana et al. 1998; Medalie et al. 1997; Ojeh et al. 2001), including type I collagen gel, fibrin gel, human plasma, and acellular human dermis. This shows that BM is not just an inert matrix that supports the epidermis, but that it also regulates epidermal morphogenesis and homeostasis via dynamic cross-talk with the overlying epidermis. Among dermal materials, acellular human dermis possesses an intact BM and supports the epidermis with good morphogenesis and a rete ridge-like pattern. The presence of pre-existing BM component proteins of the dermal matrix is essential for the development of the BM in an LSE (Ralston et al. 1999).

However, large amounts of human dermis are difficult to obtain for clinical application.

Amniotic membrane (AM) is composed of a single layer of columnar epithelial cells, a BM, an acellular compact layer, and the underlying fibroblast and spongy layers (von Versen-Hoynck et al. 2004). The BM zone underlying the amniotic epithelium resembles that of skin morphologically and ultrastructurally and consists of laminin 5 and types IV, VII, and XVII collagen (Oyama et al. 2003). As a biomaterial, AM is readily available and inexpensive and has been used to cover wounds temporarily, thereby reducing inflammation, facilitating epithelialization, and preventing scarring (Sheridan and Moreno 2001; Tseng 2001). De-epithelialized amnion has been employed as a carrier tissue for corneal or oral epithelial cell cultures to make a cornea-equivalent for ocular surface reconstruction (Nakamura et al. 2003a,b, 2004).

Since AM retains the major BM components, AM might be useful for constructing a better LSE. In this study, we have prepared de-epithelialized AM that retains the major BM components and have investigated whether AM improves the epidermis in an LSE. We have seeded keratinocytes onto AMs previously placed (epithelial side up) onto fibroblast-populated type I collagen gels, in order to construct an AM-LSE. Conventional LSEs have also been constructed from the same keratinocytes and fibroblasts by using the same protocol, except for the use of AM. We have further investigated the usefulness of AM for LSE in vitro and in vivo.

Materials and methods

Cell culture

Normal human epidermal keratinocytes (NHKs) were isolated from healthy human skin and cultured under serum-free conditions, as described previously (Shirakata et al. 2003, 2004). The cells were used for LSE cultures in their fourth passage. Fibroblasts were isolated from normal human skin and cultured in DMEM supplemented with 10% fetal calf serum (FCS), and 5th passage cells were used to construct the LSE. All procedures that involved human subjects received prior approval from the Ethics Committee of Ehime University School of Medicine, Toon, Ehime, Japan, and all subjects provided written informed consent.

Preparation of cultured skin-equivalents

The preparation of LSE has been described previously (Yang et al. 2005). Briefly, a collagen gel was prepared by mixing six volumes of ice-cold porcine collagen type I solution (Nitta Gelatin, Osaka, Japan) with one volume of 8×DMEM (Gibco), ten volumes of 1×DMEM supplemented with 20% FCS, and one volume of 0.1 N NaOH. Of this solution, 1 ml was added to each culture insert (Transwel-COL, membrane pore-size: 3 μm, Costar) in a 6-well culture plate (Costar). Following polymerization of the gel in the inserts at 37°C, two volumes of fibroblast suspension solution (5×10^5 cells/ml in 1×DMEM supplemented with 10% FCS) were added to eight volumes of the collagen solution (the final collagen concentration was 0.8 mg/ml), and then 3.5 ml of the fibroblast-containing collagen solution was applied to each insert. When the fibroblast-containing gel polymerized, DMEM supplemented with 10% FCS and ascorbic acid (final concentration: 50 ng/ml) was added. The gel was kept in submerged culture for 5 days, until the fibroblasts contracted the gel.

Human AM was obtained at cesarean section. Under sterile conditions, the AM was washed with sterile phosphate-buffered saline (PBS) and stored at −80°C in 12% dimethylsufoxide in PBS. Before use, the AM was thawed, washed three times with PBS, and cut into pieces (2.5×2.5 cm). The epithelial cells were removed from the AM by incubation in 0.02% EDTA at 37°C for 2 h and then gentle scraping with a cell scraper under a microscope. The spongy layer was also removed. The complete removal of the epithelial cells was confirmed by using hematoxylin and eosin (HE) staining.

The de-epithelialized AM was put, epithelial side up, onto the contracted gel surface, and a stainless steel ring (interior diameter: 11 mm) was overlaid on it to stabilize it. In the hole of the ring, 4×10^5 keratinocytes in 100 μl MCDB 153 type II were seeded onto the AM. The keratinocytes were maintained, submerged in culture, for 2 days. When the keratinocytes reached confluence, the LSE was lifted to the air-liquid interface and cornification medium (a 1:1 mixture of Ham's F-12 and DMEM supplemented with 2% FCS and other supplements; see Yang et al. 2005) was added. The medium was changed every other day. To construct a conventional LSE, keratinocytes were seeded onto the contracted gel and then submerged and airlifted as described above, except for the use of de-epithelialized AM. The stainless steel rings were used to adjust the seeding cell density. Both types of LSE were harvested 7 and 21 days after airlifting. For HE staining, the LSE was fixed in 20% formalin and embedded in paraffin. For immunohistochemical staining, the LSE was snap-frozen in OCT compound. We performed more than 20 experiments, with similar results being obtained in each (a representative experiment is shown in the figures). In comparative studies, keratinocytes and fibroblasts from the same donor were used.

Histology and immunohistochemical staining

Paraffin-embedded LSE samples were sectioned at 6 μm and stained with HE. For immunohistochemical staining, a Histofine Simple Stain MAX-PO (M) kit (Nichirei, Tokyo, Japan) was used according to the manufacturer's instructions. Frozen sections (7 μm) were first incubated with 0.3% hydrogen peroxide for 30 min to remove endogenous peroxidase activity and then incubated with primary antibodies at appropriate dilutions (Table 1) overnight at 4°C. The sections were incubated with enzyme-conjugated

secondary antibodies for 30 min at room temperature and then with the staining substrate. Images were obtained by using an Olympus AX80 microscope coupled with an Olympus DP50 digital camera (Olympus, Tokyo, Japan). We performed at least three independent studies and obtained similar results (a representative experiment is shown in the figures).

Evaluating the epidermal spreading potential of AM-LSEs

Stainless steel rings with an inner diameter of 6 mm were put on gels with or without AM, and 2×10^5 keratinocytes in 30 µl of MCDB 153 II medium were seeded in the hole of each ring. When the keratinocytes reached confluence, the LSEs were lifted to the air-liquid surface, and the stainless steel rings were removed. At days 0, 3, 5, 7, and 10 after being airlifted, epidermal size was measured by using a computer-assisted morphometric analysis. The epidermal size of the conventional and AM-LSEs was compared statistically by using Student's *t*-test.

Transplanting cultured LSEs

The animal grafting protocol was approved by the Ethics Committee of Ehime University School of Medicine. Eight-week-old female BALB/cAJcl-nu nude mice were anesthetized by intraperitoneal injection of 0.3 ml of Avertin (1.25% tribromoethanol, 2.5% 2-methyl-2-butanol solution). Full-thickness wounds were created on the skin of the backs of each mouse by using an 8-mm skin biopsy punch. A piece of AM-LSE or conventional LSE of matching size (7 days after airlift) obtained using the same punch was grafted onto the wound and covered with a transparent film. At 14 days after transplantation, the grafts were harvested. One part of each graft was paraffin-embedded and sectioned at 6 µm. Some sections were stained with HE, and some were de-paraffinized and blocked for endogenous peroxidase activity and then blood vessels were stained with rabbit antibody against type IV collagen (at dilution 1:50; American Research Products, Belmont, Mass.) according to the protocol of the Histofine SAB-AP (R) kit (Nichirei, Tokyo, Japan). Finally, the sections were counterstained with hematoxylin for cell nuclei. One part of each graft was also processed for electron-microscopic analysis. We performed at least three independent studies and obtained similar results (a representative experiment is shown in the figures).

Transmission electron microscopy

Specimens were fixed with 0.1% tannic acid, 2.5% glutaraldehyde in 0.1 M phosphate buffer (pH 7.4) for 2 h, washed with phosphate buffer, postfixed with 1% osmium tetroxide in phosphate buffer for 2 h, washed with 0.25 M sucrose solution, dehydrated in a graded series of ethanol, and embedded in an Epon-resin mixture. Ultrathin sections (<60–80 nm) were prepared by using a Leica Ultracut S, double-stained with uranyl acetate and lead citrate, and examined with a transmission electron microscope (JEM-1230, JEOL, Tokyo, Japan) at 80 kV.

Results

AM-LSE has a better-organized and more mature epidermis

Both AM-LSE and the conventional LSE showed differentiated epidermis with a basal layer, suprabasal layer, and stratum corneum at days 7 and 21 after airlifting (Fig. 1). The epidermal stratification was however better organized in the AM-LSE; the basal cells were cuboid, smaller, and more compact, and aligned along the AM with clear demarcation (Fig. 1a,b). In the conventional LSE, the epidermal stratification was not as well organized. The larger round basal cells were sparsely aligned along the dermal-epidermal junction, and the number of basal cells had decreased considerably by day 21 (Fig. 1e,f).

We found keratin 6, a marker of keratinocyte activation, only in hair follicles in normal human skin sections (Fig. 2). In AM-LSE, keratin 6 staining was faint at day 7 and disappeared almost completely in the basal and lower suprabasal layers by day 21 (Fig. 2a,k). In conventional LSE, the epidermis strongly expressed keratin 6 up to

Table 1 Details of primary antibodies used

Antigen	Clone	Dilution of antibody	Antibody source
E-cadherin	HECD-1	1:100	TaKaRa
Desmoglein 1	27B2	1:100	Zymed
Desmoglein 3	5G11	1:100	Zymed
Keratin 10	LHP1	1:100	NeoMarkers
Keratin 6	LHK6B	1:100	NeoMarkers
Integrin β4	3E1	1:100	Chemicon
Integrin α6	6B4	1:100	Chemicon
Collagen VII	LH7:2	1:100	NeoMarkers
Collagen IV	2311C3	1:200	Chemicon
Laminin 5	GB3	1:100	Sera-lab

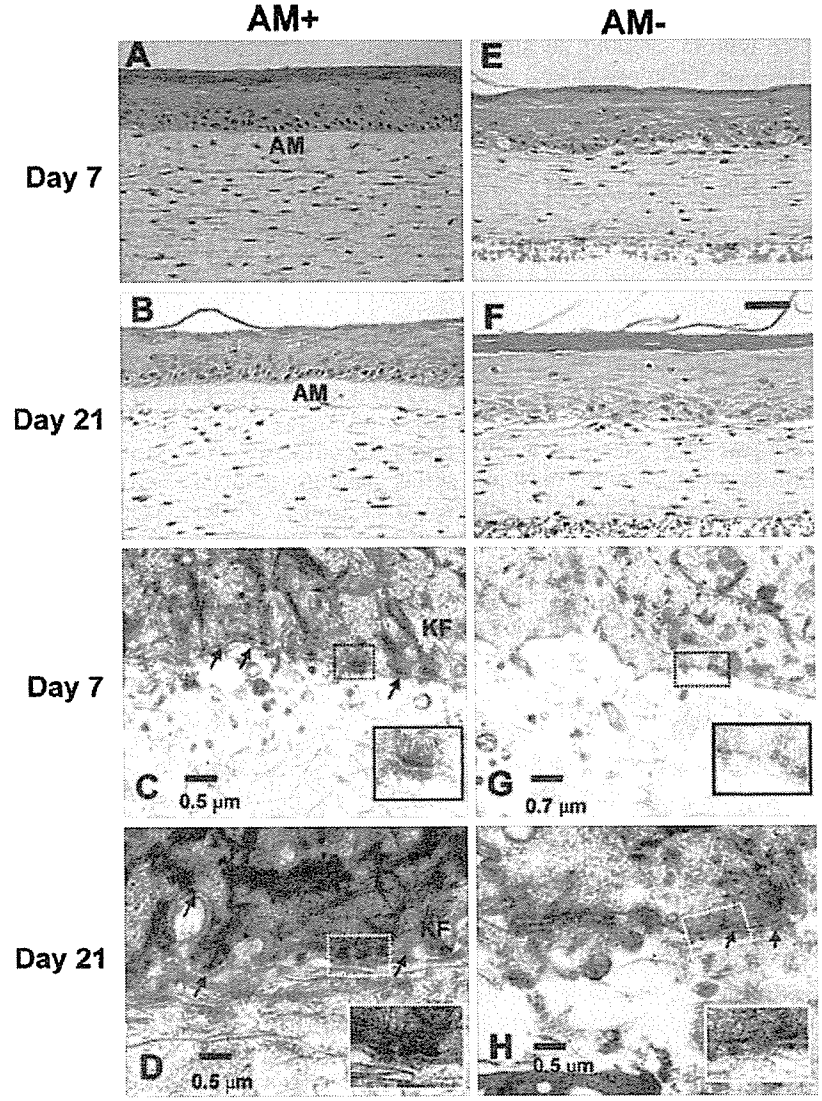

Fig. 1 Morphology of the epidermis and basement membrane (BM) in living skin-equivalent derived from amniotic membrane (AM-LSE; *AM+*) and in conventional LSE (*AM−*). Samples were harvested at days 7 (**a**, **e**, **c**, **g**) and 21 (**b**, **f**, **d**, **h**) from AM-LSE (**a**, **b**, **c**, **d**) and conventional LSE (**e**, **f**, **g**, **h**). Hematoxylin and eosin (HE) staining (**a**, **b**, **e**, **f**) showed a better-stratified epidermis with more compact, columnar basal cells in AM-LSEs. Transmission electron microscopy (**c**, **d**, **g**, **h**) revealed a more continuous lamina densa (*arrows*) and better-developed hemidesmosomes (*insets*) in the AM-LSEs than in the conventional LSEs (*KF* keratin filaments). *Bars* 50 μm (**a**, **b**, **e**, **f**), 0.5 μm (**c**, **d**, **h**), 0.7 μm (**g**)

day 21 after airlifting (Fig. 2f,p). In AM-LSE, keratin 10 expression increased with time, and by day 21, keratin 10 was distributed from the suprabasal layer to the stratum corneum, in a pattern similar to that of normal human skin (Fig. 2b,l). By contrast, keratin 10 expression decreased at day 7 and was barely observed at day 21 in the conventional LSE (Fig. 2g,q). In both LSE models, cell-cell junctions were well developed in similar patterns, as documented by the strongly expressed cell-cell junction proteins, such as E-cadherin (Fig. 2c,h,m,r), desmoglein 1 (Fig. 2d,i,n,s), and desmoglein 3 (Fig. 2e,j,o,t).

Presence of de-epithelialized AM enhances development of BM and hemidesmosomes in LSE

Types IV and VII collagen were present in de-epithelialized AM (data not shown). In the AM-LSE, immunohistochemical staining for types IV and VII collagen was seen along the epidermal-dermal junction at 7 days after airlifting (Fig. 3a,b). The type IV collagen staining was more intense at day 21 (Fig. 3k), whereas less collagen VII was observed (Fig. 3l). In conventional LSE at day 7, only small amounts of collagen IV and VII were noted along the epidermal-dermal junction (Fig. 3f,g), and although the staining increased, it still appeared minimal at day 21 (Fig. 3p,q).

The assembly of the BM was also characterized by determining the distribution of laminin 5 and its receptor, α6β4 integrin. BM normalization could be assessed by the degree to which these proteins were deposited in a polarized linear pattern at the BM zone (Andriani et al. 2003). In AM-LSE, laminin 5 was deposited linearly and was polarized along the epidermal-dermal junction at day 7 (Fig. 3c); the staining intensity had increased by day 21 (Fig. 3m). By contrast, in conventional LSE, little laminin 5 was seen at day 7 (Fig. 3h); by day 21, although more laminin 5 was expressed, its localization was discontinuous and patchy at the suprabasal layer (Fig. 3r). The receptor, α6β4 integrin, was distributed in a pattern similar to that of

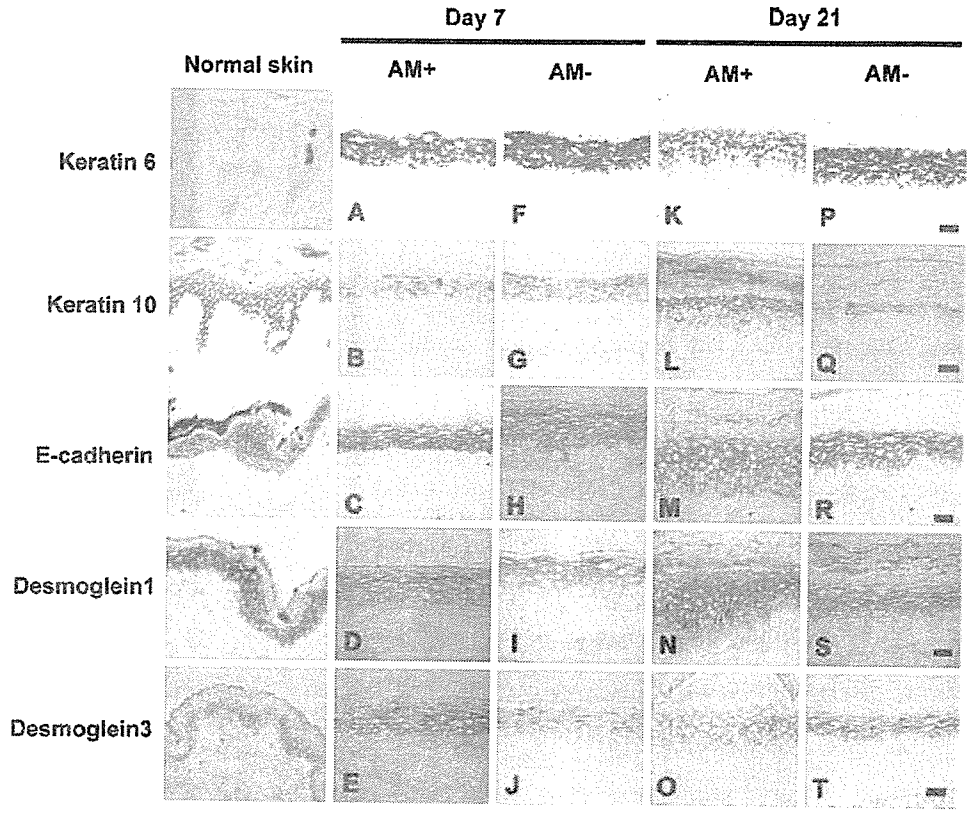

Fig. 2 Keratin and cell-cell junction protein expression in AM-LSE (*AM+*) and conventional LSE (*AM−*). Samples from days 7 (**a-j**) and 21 (**k-t**) from AM-LSEs (**a-e**, **e-o**) and conventional LSEs (**f-j**, **p-t**) were processed for immunohistochemical analysis. The expression of keratin 6 (**a**, **f**, **k**, **p**), keratin 10 (**b**, **g**, **l**, **q**), E-cadherin (**c**, **h**, **m**, **r**), desmoglein 1 (**d**, **i**, **n**, **s**), and desmoglein 3 (**e**, **j**, **o**, **t**) was determined by using the respective monoclonal antibodies. *Bars* 50 μm

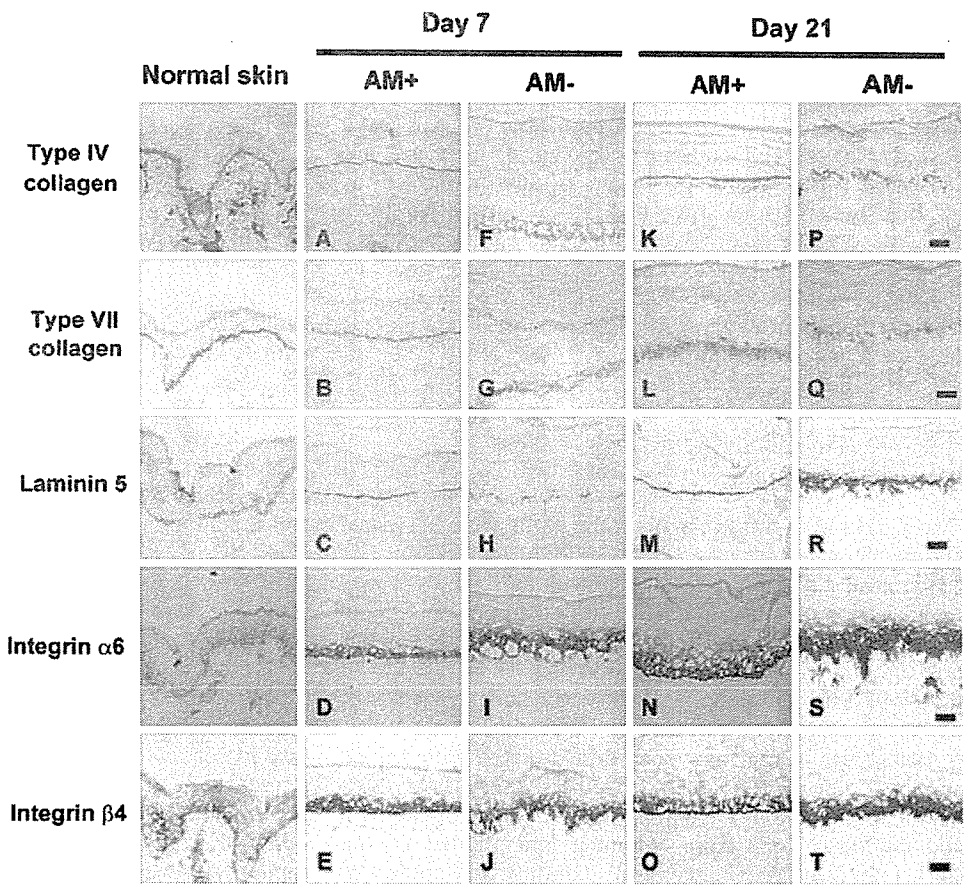

Fig. 3 Integrin and BM component expression in AM-LSE (*AM+*) and conventional LSE (*AM−*). Samples of AM-LSE (**a-e**, **k-o**) and conventional LSE (**f-j**, **p-t**) cultured for 7 (**a-j**) or 21 days (**k-t**) were stained immunohistochemically with monoclonal antibodies against type IV collagen (**a**, **f**, **k**, **p**), type VII collagen (**b**, **g**, **l**, **q**), laminin 5 (**c**, **h**, **m**, **r**), integrin α6 (**d**, **i**, **n**, **s**), and integrin β4 (**e**, **j**, **o**, **t**). *Bars* 50 μm

laminin 5. In AM-LSE, both α6 and β4 integrin subunits were restricted to the basal pole of the basal cells at days 7 and 21 (Fig. 3d,n,e,o). In conventional LSE, α6 and β4 integrin proteins were synthesized and accumulated in the epidermis; they were distributed predominantly in the suprabasal layer and did not localize in a linear pattern (Fig. 3i,s,j,t).

The development of the BM zones of the LSEs was further elucidated by using transmission electron microscopy (TEM) (Fig. 1c,d,g,h). At day 7, a continuous lamina densa was formed along the plasma membrane of the keratinocytes, with many hemidesmosomes, in the AM-LSE. The hemidesmosomes were well developed structurally, with inner and outer plaques clearly being distinguished; keratin filaments were connected to the inner plaques (Fig. 1c), whereas in the conventional LSE, little lamina densa or BM structures were seen at day 7. Along the plasma membrane of the basal cells, some electron-dense hemidesmosome-like structures were seen; however, they did not possess the structural features of hemidesmosomes (Fig. 1g). At day 21, the lamina densa and hemidesmosomes in the AM-LSE were well developed, and the structural features of hemidesmosomes were clearly displayed (Fig. 1d), whereas in conventional LSE, an interrupted lamina densa was seen, with poorly developed hemidesmosomes (Fig. 1h).

De-epithelialized AM improved epidermal outgrowth

On the day of airlifting (day 0), the epidermis of both the AM-LSE and conventional LSE was 6 mm in diameter. The epidermis of the AM-LSE continued to outgrow faster than that of the conventional LSE (Fig. 4): at day 3, the epidermis measured 7.7±0.4 mm (it had increased by 28.3%), and at day 10, it reached 18.3±1.1 mm (over three times its original size). By contrast, the epidermis of the conventional LSE did not change in size by day 3, and only a 78.3% increase to 10.7±0.2 mm was seen at day 10. These results indicated that the AM stimulated keratinocyte migration and proliferation.

AM-LSE grafts on nude mice exhibit better morphogenesis of the epidermis and BM

Two weeks after transplantation, the grafts were harvested and manipulated for observation by light microscopy and TEM. Both the AM-LSE and conventional LSE took well on the recipient nude mice. The fibroblast-populated gel in conventional LSE was prone to separate from the epidermis and was fragile during manipulation. The epidermis of the AM-LSE was tightly attached to the underlying tissue, and the graft was more resistant to rupture. The epidermis of both types of graft was well differentiated with a thick stratum corneum (Fig. 5a,b). The epidermis of the AM-LSE was better stratified than that of the conventional LSE, and the basal cells were columnar and aligned on the surface of the AM (Fig. 5a). By contrast, the epidermal

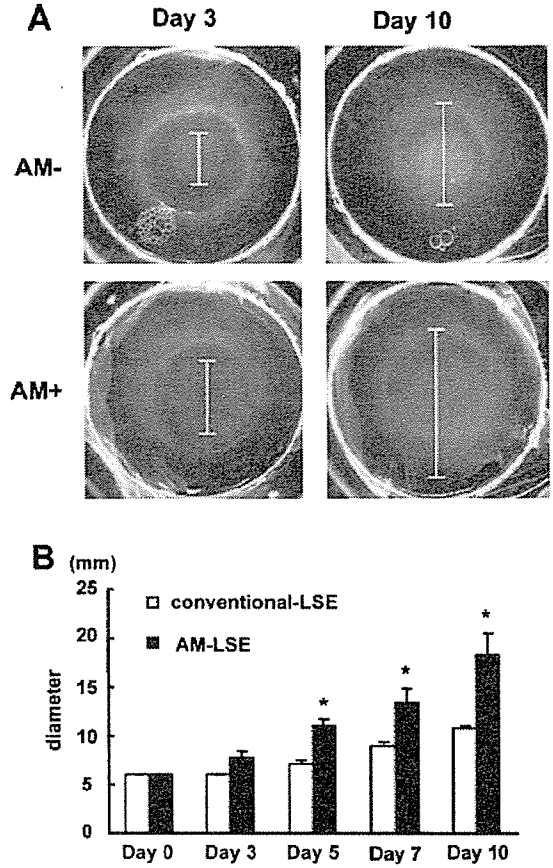

Fig. 4 Comparison of epidermal outgrowth of AM-LSE and conventional LSE. **a** Stainless steel rings with an inner diameter of 6 mm were placed on gels with (*AM+*) or without (*AM−*) AM, and 2×10^5 keratinocytes were seeded. When the keratinocytes reached confluence, the LSEs were lifted to the air-liquid surface, and the stainless steel rings were removed. Epidermal size (*lines*) was monitored after airlifting. **b** The epidermal diameter of AM-LSE and conventional LSE was measured at days 3, 5, 7, and 10, and the mean value for each day was calculated (n=3, $^*P<0.05$)

stratification in the conventional LSE was disorganized, with few basal cells along the dermal-epidermal junction (Fig. 5b).

In the AM- LSE graft, an electron-lucent lamina lucida was clearly observed between the basal cell plasma membrane and the continuous electron-dense lamina densa. Hemidesmosomes were well developed structurally and dotted along the plasma membrane of the basal cells (Fig. 5c). By contrast, the BM in the conventional LSE graft was rudimentary and faint, and far fewer hemidesmosomes were present than in the AM-LSE graft, as seen in vitro (Fig. 5d).

The basal cell number per millimeter in three separate fields of view of both LSE grafts was calculated and showed a significantly higher cell number in AM-LSEs than in conventional LSEs (Fig. 5h). Since vascularization is essential for graft survival, we investigated the angiogenesis in AM-LSE and conventional LSE. We found the AM-LSE grafts were better vascularized, with even some capillaries infiltrating into the AM (Fig. 5e), whereas blood

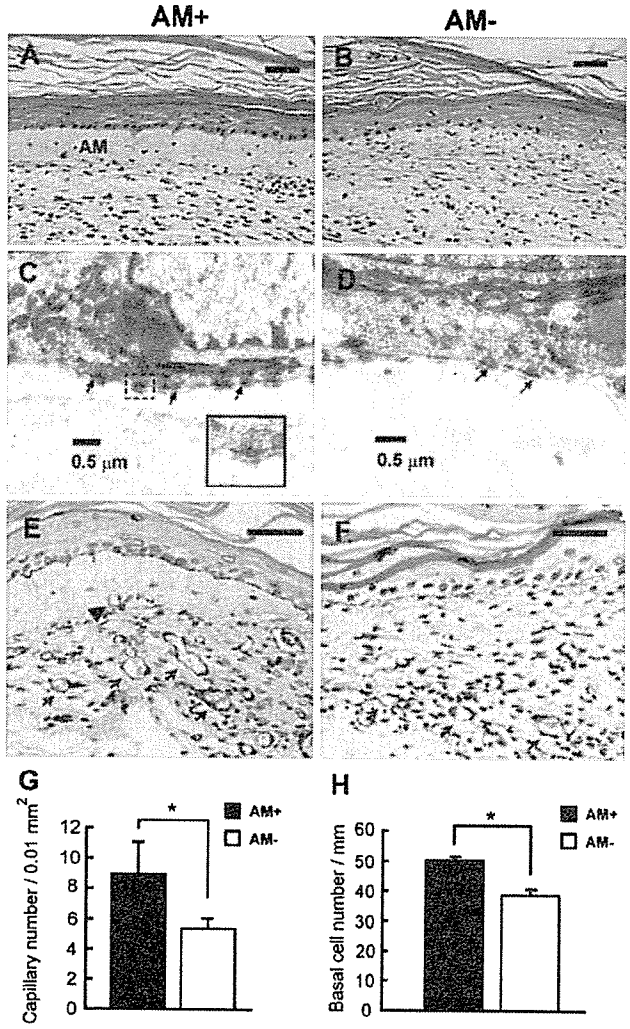

Fig. 5 Light-microscopic and ultrastructural views of AM-LSE (*AM+*) and conventional LSE (*AM−*) in vivo. AM-LSE or conventional LSE was grafted onto the back skin of nude mice. Two weeks after transplantation, samples were harvested and processed for HE staining (**a**, **b**), TEM (**c**, **d**), and immunohistochemical staining for type IV collagen to detect blood vessels (**e**, **f**). HE staining showed better organized epidermis (**a**, **b**) and more basal cells (**h**) in AM-LSE grafts than in conventional LSE grafts. TEM revealed a continuous lamina densa (*arrows* in **c**) with many structurally well-developed hemidesmosomes (*inset* in **c**) in the AM-LSE, and a faint interrupted lamina densa (*arrows* in **d**) with fewer, poorly developed hemidesmosomes in the conventional LSE. More blood vessels (*arrows* in **e**, **f**) were found in AM-LSE grafts than in conventional LSE grafts (**e**, **f**, **g**), with some vessels infiltrating into the AM (*arrowhead* in **e**). **P*<0.05 (**g**, **h**). *Bars* 50 μm (**a**, **b**, **e**, **f**), 0.5 μm (**c**, **d**)

vessels were fewer in conventional LSE grafts (Fig. 5f). The number of blood vessels/0.01 mm^2 in three separate fields of view was calculated and revealed significantly more blood vessels in AM-LSE grafts than in conventional LSE (Fig. 5g).

Discussion

Epithelial-mesenchymal interactions play important roles in controlling epidermal morphogenesis and homeostasis. The interaction between keratinocytes and the insoluble BM proteins contributes to the maintenance of tissue architecture and affects various biological processes, such as cell attachment, proliferation, differentiation, and migration (Blomme et al. 1998; Kim et al. 1994). In autologous split-thickness skin grafting for treating deep burns, a disturbance in BM reassembly is believed to be responsible for post-burn blisters (Bergman et al. 1997). In conventional LSEs constructed by seeding keratinocytes on a fibroblast-populated type I collagen gel, the BM is not well developed a few weeks after airlifting and is rarely seen after their transplantation onto nude mice (Amano et al. 2001; Medalie et al. 1997).

During the construction of a LSE, pre-existing BM components on the dermal matrix contribute to improving the morphology of the epidermis and are necessary for the formation of hemidesmosomes and the development of a lamina densa (Kim et al. 2001; Medalie et al. 1997; Ralston et al. 1999). The de-epithelialized AM is immunohistochemically positive for types VII and IV collagen, but negative for laminin 5 (data not shown), which is probably lost during the EDTA treatment and subsequent mechanical scraping used to remove epithelial cells from the AM. In this study, we have constructed LSEs with or without de-epithelialized AM to investigate the usefulness of AM. The same types of keratinocytes and fibroblasts and the same techniques have been used for both types of LSE in order to elucidate the roles of de-epithelialized AM in epidermal morphology, BM development, and epidermal migration. We have compared the two types of LSE morphologically, immunohistochemically, and ultrastructurally.

The results indicate that the presence of certain BM components on de-epithelialized AM improve the epidermogenesis of the overlaying epidermis, which is more mature and better organized than epidermis without AM. Similar effects of BM proteins have also been documented in a composite skin-equivalent by using, as the substrate, acellular dermis, which retains several key BM components (Medalie et al. 1997; Ralston et al. 1999). The sustained growth of the keratinocytes in an LSE is maintained by a well-developed BM (Andriani et al. 2003), whose formation is facilitated by the pre-existing BM components.

Laminin 5 is also essential for epidermal-dermal adhesion. Laminin 5 bridges integrin $\alpha6\beta4$ with underlying connective tissue through an association with laminin 6 and 7 and direct binding to type VII collagen (Champliaud et al. 1996; Rousselle et al. 1997). The effect of pre-existing BM components in normalizing the deposition and polarization of laminin 5 has been documented in the construction of LSE by seeding keratinocytes on de-epithelialized dermis (Andriani et al. 2003, 2004). Moreover, the presence of laminin 5 initiates hemidesmosome formation and accelerates the formation of the lamina densa (Nishiyama et al. 2000; Tsunenaga et al. 1998). The de-epithelialized AM

also enhances the polarized basal distribution of α6β4 integrin along the dermal-epidermal junction, as compared with the more suprabasal, albeit denser, distribution in conventional LSEs.

The well-developed basal lamina and hemidesmosomes and the polarized basal deposition of laminin 5 and α6β4 integrin guarantee a stable association between the epidermis and the underlying tissues in AM-LSEs. This might explain why the epidermis is more resistant to separation from the underlying connective tissue during the manipulation of AM-LSEs, as compared with the loose connection in conventional LSEs.

The outgrowth of corneal explants has been reported to be faster on de-epithelialized AM than on intact AM; this implies that the exposed extracellular matrix of de-epithelialized AM is more inducive to epithelial cell migration (Koizumi et al. 2000). Of the BM components, collagen IV had been shown to assist keratinocyte migration through an interaction with keratinocyte α2β1 integrin (Kim et al. 1994). In AM-LSEs, the epidermis outgrows much faster than when on a fibroblast-populated type I collagen gel; AM-LSEs might thus better meet the clinical need to provide a skin-equivalent for a larger area in a shorter time.

AM-LSE therefore appears superior to conventional LSE in several ways (see above). We have transplanted AM-LSE and conventional LSE onto nude mice and found that both LSEs take well on full-thickness wounds of nude mice. A better-organized epidermis, continuous lamina densa and lamina lucida, better-formed hemidesmosomes, and more importantly, better vascularization are seen with AM-LSE. When manipulating the graft for transplantation, the AM-LSE is much more resistant to rupture, as compared with the fragile conventional LSE.

However, the lack of the BM zone in conventional LSE can be supplemented not only by the epidermal side of the de-epithelialized amnion, but also by the stromal side of the amnion, which can support the growth of fibroblasts (Espana et al. 2003; Kumar et al. 2003). This implies that amnion could provide a scaffold for LSE, greatly simplifying the procedures for making dermal matrix and avoiding the use of animal collagen, which is costly and ethically problematic. Moreover, the limited immunogenicity and immune-privilege of amnion (Kubo et al. 2001; Mahgoub et al. 2004), together with its anti-inflammatory effects (Park and Tseng 2000), make it a suitable material for transplantation and a biological immune barrier for xenotransplantation, which may facilitate allograft transplantation of AM-LSE. Amnion can be readily obtained from cesarean delivery under screening for viral diseases and can also be sterilized and preserved at low cost for long periods without obvious architectural changes (Ravishanker et al. 2003; Rejzek et al. 2001; von Versen-Hoynck et al. 2004), thereby ensuring the plentiful supply of amnion in clinical application. Usually, we can take five to six pieces of amnion of 40–50 mm in size in one delivery. Amnion of this size is easily manipulated, fits the commonly used transwell culture insert (diameter: 75 mm), and can be tailored and used in one piece to cover fresh wounds or made into mesh grafts or stamp grafts to cover granulation tissue as split skin grafts.

In conclusion, the AM-LSE had good epidermal morphology and a well-developed BM zone and is easy to manipulate during transplantation. Since AM is readily obtainable, and since a large amount of AM can be supplied compared with other materials, an AM-LSE should be a good skin substitute for treating burns, ulcers, and other skin defects.

Acknowledgements We thank Teruko Tsuda, Eriko Tan, and Wakana Itoh for technical assistance.

References

Amano S, Akutsu N, Matsunaga Y, Nishiyama T, Champliaud MF, Burgeson RE, Adachi E (2001) Importance of balance between extracellular matrix synthesis and degradation in basement membrane formation. Exp Cell Res 271:249–262

Andriani F, Margulis A, Lin N, Griffey S, Garlick JA (2003) Analysis of microenvironmental factors contributing to basement membrane assembly and normalized epidermal phenotype. J Invest Dermatol 120:923–931

Andriani F, Garfield J, Fusenig NE, Garlick JA (2004) Basement membrane proteins promote progression of intraepithelial neoplasia in 3-dimensional models of human stratified epithelium. Int J Cancer 108:348–357

Bergman R, David R, Ramon Y, Ramon M, Kerner H, Kilim S, Peled I, Friedman-Birnbaum R (1997) Delayed postburn blisters: an immunohistochemical and ultrastructural study. J Cutan Pathol 24:429–433

Blomme EA, Weckmann MT, Capen CC, Rosol TJ (1998) Influence of extracellular matrix macromolecules on normal human keratinocyte phenotype and parathyroid hormone-related protein secretion and expression in vitro. Exp Cell Res 238: 204–215

Champliaud MF, Lunstrum GP, Rousselle P, Nishiyama T, Keene DR, Burgeson RE (1996) Human amnion contains a novel laminin variant, laminin 7, which like laminin 6, covalently associates with laminin 5 to promote stable epithelial-stromal attachment. J Cell Biol 132:1189–1198

Eaglstein WH, Falanga V (1998) Tissue engineering and the development of Apligraf a human skin equivalent. Adv Wound Care 11:1–8

Espana EM, He H, Kawakita T, Di Pascuale MA, Raju VK, Liu CY, Tseng SC (2003) Human keratocytes cultured on amniotic membrane stroma preserve morphology and express keratocan. Invest Ophthalmol Vis Sci 44:5136–5141

Guerret S, Govignon E, Hartmann DJ, Ronfard V (2003) Long-term remodeling of a bilayered living human skin equivalent (Apligraf) grafted onto nude mice: immunolocalization of human cells and characterization of extracellular matrix. Wound Repair Regen 11:35–45

Kim JP, Chen JD, Wilke MS, Schall TJ, Woodley DT (1994) Human keratinocyte migration on type IV collagen. Roles of heparin-binding site and alpha 2 beta 1 integrin. Lab Invest 71:401–408

Kim SW, Park KC, Kim HJ, Cho KH, Chung JH, Kim KH, Eun HC, Lee JS, Park KD (2001) Effects of collagen IV and laminin on the reconstruction of human oral mucosa. J Biomed Mater Res 58:108–112

Koizumi N, Fullwood NJ, Bairaktaris G, Inatomi T, Kinoshita S, Quantock AJ (2000) Cultivation of corneal epithelial cells on intact and denuded human amniotic membrane. Invest Ophthalmol Vis Sci 41:2506–2513

Kubo M, Sonoda Y, Muramatsu R, Usui M (2001) Immunogenicity of human amniotic membrane in experimental xenotransplantation. Invest Ophthalmol Vis Sci 42:1539–1546

Kumar TR, Shanmugasundaram N, Babu M (2003) Biocompatible collagen scaffolds from a human amniotic membrane: physicochemical and in vitro culture characteristics. J Biomater Sci Polym Ed 14:689–706

Llames SG, Del Rio M, Larcher F, Garcia E, Garcia M, Escamez MJ, Jorcano JL, Holguin P, Meana A (2004) Human plasma as a dermal scaffold for the generation of a completely autologous bioengineered skin. Transplantation 77:350–355

Mahgoub MA, Ammar A, Fayez M, Edris A, Hazem A, Akl M, Hammam O (2004) Neovascularization of the amniotic membrane as a biological immune barrier. Transplant Proc 36: 1194–1198

Meana A, Iglesias J, Del Rio M, Larcher F, Madrigal B, Fresno MF, Martin C, San Roman F, Tevar F (1998) Large surface of cultured human epithelium obtained on a dermal matrix based on live fibroblast-containing fibrin gels. Burns 24:621–630

Medalie DA, Eming SA, Collins ME, Tompkins RG, Yarmush ML, Morgan JR (1997) Differences in dermal analogs influence subsequent pigmentation, epidermal differentiation, basement membrane, and rete ridge formation of transplanted composite skin grafts. Transplantation 64:454–465

Nakamura T, Endo K, Cooper LJ, Fullwood NJ, Tanifuji N, Tsuzuki M, Koizumi N, Inatomi T, Sano Y, Kinoshita S (2003a) The successful culture and autologous transplantation of rabbit oral mucosal epithelial cells on amniotic membrane. Invest Ophthalmol Vis Sci 44:106–116

Nakamura T, Koizumi N, Tsuzuki M, Inoki K, Sano Y, Sotozono C, Kinoshita S (2003b) Successful regrafting of cultivated corneal epithelium using amniotic membrane as a carrier in severe ocular surface disease. Cornea 22:70–71

Nakamura T, Yoshitani M, Rigby H, Fullwood NJ, Ito W, Inatomi T, Sotozono C, Nakamura T, Shimizu Y, Kinoshita S (2004) Sterilized, freeze-dried amniotic membrane: a useful substrate for ocular surface reconstruction. Invest Ophthalmol Vis Sci 45:93–99

Nishiyama T, Amano S, Tsunenaga M, Kadoya K, Takeda A, Adachi E, Burgeson RE (2000) The importance of laminin 5 in the dermal-epidermal basement membrane. J Dermatol Sci 24: S51–S59

Ojeh NO, Frame JD, Navsaria HA (2001) In vitro characterization of an artificial dermal scaffold. Tissue Eng 7:457–472

Oyama N, Bhogal BS, Carrington P, Gratian MJ, Black MM (2003) Human placental amnion is a novel substrate for detecting autoantibodies in autoimmune bullous diseases by immunoblotting. Br J Dermatol 148:939–944

Park WC, Tseng SC (2000) Modulation of acute inflammation and keratocyte death by suturing, blood, and amniotic membrane in PRK. Invest Ophthalmol Vis Sci 41:2906–2914

Ralston DR, Layton C, Dalley AJ, Boyce SG, Freedlander E, MacNeil S (1999) The requirement for basement membrane antigens in the production of human epidermal/dermal composites in vitro. Br J Dermatol 140:605–615

Ravishanker R, Bath AS, Roy R (2003) "Amnion Bank"—the use of long term glycerol preserved amniotic membranes in the management of superficial and superficial partial thickness burns. Burns 29:369–374

Rejzek A, Weyer F, Eichberger R, Gebhart W (2001) Physical changes of amniotic membranes through glycerolization for the use as an epidermal substitute. Light and electron microscopic studies. Cell Tissue Bank 2:95–102

Rousselle P, Keene DR, Ruggiero F, Champliaud MF, Rest M, Burgeson RE (1997) Laminin 5 binds the NC-1 domain of type VII collagen. J Cell Biol 138:719–728

Sheridan RL, Moreno C (2001) Skin substitutes in burns. Burns 27:92

Shirakata Y, Tokumaru S, Yamasaki K, Sayama K, Hashimoto K (2003) So-called biological dressing effects of cultured epidermal sheets are mediated by the production of EGF family, TGF-beta and VEGF. J Dermatol Sci 32:209–215

Shirakata Y, Ueno H, Hanakawa Y, Kameda K, Yamasaki K, Tokumaru S, Yahata Y, Tohyama M, Sayama K, Hashimoto K (2004) TGF-beta is not involved in early phase growth inhibition of keratinocytes by 1alpha,25(OH)2vitamin D3. J Dermatol Sci 36:41–50

Tseng SC (2001) Amniotic membrane transplantation for ocular surface reconstruction. Biosci Rep 21:481–489

Tsunenaga M, Adachi E, Amano S, Burgeson RE, Nishiyama T (1998) Laminin 5 can promote assembly of the lamina densa in the skin equivalent model. Matrix Biol 17:603–613

von Versen-Hoynck F, Syring C, Bachmann S, Moller DE (2004) The influence of different preservation and sterilisation steps on the histological properties of amnion allografts-light and scanning electron microscopic studies. Cell Tissue Bank 5:45–56

Yang L, Shirakata Y, Tamai K, Dai X, Hanakawa Y, Tokumaru S, Yahata Y, Tohyama M, Shiraishi K, Nagai H, Wang X, Murakami S, Sayama K, Kaneda Y, Hashimoto K (2005) Microbubble-enhanced ultrasound for gene transfer into living skin equivalents. J Dermatol Sci 40:105–114

THE JOURNAL OF BIOLOGICAL CHEMISTRY VOL. 281, NO. 19, pp. 13209–13216, May 12, 2006

A Novel Function of Angiotensin II in Skin Wound Healing

INDUCTION OF FIBROBLAST AND KERATINOCYTE MIGRATION BY ANGIOTENSIN II VIA HEPARIN-BINDING EPIDERMAL GROWTH FACTOR (EGF)-LIKE GROWTH FACTOR-MEDIATED EGF RECEPTOR TRANSACTIVATION

Received for publication, September 6, 2005, and in revised form, March 16, 2006 Published, JBC Papers in Press, March 16, 2006, DOI 10.1074/jbc.M509771200

Yoko Yahata[‡1], Yuji Shirakata[‡1,2], Sho Tokumaru[‡], Lujun Yang[‡], Xiuju Dai[‡], Mikiko Tohyama[‡], Teruko Tsuda[‡], Koji Sayama[‡], Masaru Iwai[§], Masatsugu Horiuchi[§], and Koji Hashimoto[‡]

From the [‡]Department of Dermatology and the [§]Division of Medical Biochemistry and Cardiovascular Biology, Ehime University School of Medicine, Shitsukawa, Toon, Ehime 791-0295, Japan

The role of angiotensin II (Ang II) in the control of systemic blood pressure and volume homeostasis is well known and has been extensively studied. Recently, Ang II was suggested to also have a function in skin wound healing. In the present study, the *in vivo* function of Ang II in skin wound healing was investigated using Ang II type 1 receptor (AT1R) knock-out mice. Wound healing in these mice was found to be markedly delayed. Keratinocytes and fibroblasts play important roles in wound healing, and thus the effect of Ang II on the migration of these cells was examined. Ang II stimulated keratinocyte and fibroblast migration in a dose-dependent manner. It has been reported that G protein-coupled receptor (GPCR) activation induces epidermal growth factor (EGF) receptor (EGFR) transactivation through the shedding of heparin-binding EGF-like growth factor (HB-EGF). As AT1R is a GPCR, it was hypothesized that Ang II-induced keratinocyte and fibroblast migration is mediated by EGFR transactivation. Ang II induced EGFR phosphorylation, which was inhibited by an AT1R antagonist, HB-EGF neutralizing antibody, and an HB-EGF antagonist in both keratinocytes and in fibroblasts. Moreover, Ang II-induced migration of keratinocytes and fibroblasts was also prevented by these inhibitors. Taken together, these findings clearly demonstrate, for the first time, that Ang II plays an important role in skin wound healing and that it functions by accelerating keratinocyte and fibroblast migration in a process mediated by HB-EGF shedding.

Cutaneous wound healing requires precise coordination of epithelialization, dermal repair, and angiogenesis (1). In turn, epithelialization is ultimately dependent on the migratory, proliferative, and differentiation abilities of keratinocytes, while dermal repair requires the production of extracellular matrix by fibroblasts. The growth and differentiation of these two cell types are regulated by several different growth factors (2).

The vasoactive octapeptide angiotensin II (Ang II)[3] has a well described role in the control of systemic blood pressure and volume homeostasis. In the rat, both cardiac and skin fibroblasts express Ang II receptors, which have been shown to be involved in cell growth and the activation of second messenger pathways, such as the mobilization of intracellular calcium (3, 4). In addition, Ang II was shown to act as a mitogen for smooth muscle cells, fibroblasts, and endothelial cells (5–10). Mammalian cells express two types of Ang II receptors, Ang II type 1 receptor (AT1R) and Ang II type 2 receptor (AT2R) (11). Most of the known biological effects of Ang II are mediated through AT1R, a G protein-coupled receptor (GPCR) that is expressed in a wide variety of cells and tissues. In mouse, there are two isoforms of AT1R, AT1aR and AT1bR. AT1R has been shown to mediate mitogenesis in cardiac fibroblasts and vascular smooth muscle cells (12, 13), whereas in fibroblasts, the activation of AT2R has two opposing effects, inhibition of cell growth (14, 15) and promotion of apoptosis (16). Thus, the balance between the expressions of these two receptor types may be crucial in determining the response to Ang II. The integral role of Ang II in regulating systemic blood pressure and volume homeostasis is well known and has been extensively studied. In the present study, we show that Ang II is also involved in wound repair.

Recent investigations demonstrated that the stimulation of GPCR induces shedding of epidermal growth factors (EGF) via the activation of a disintegrin and metalloprotease (ADAM), followed by transactivation of the EGF receptor (EGFR). HB-EGF, an EGF family member, is thought to play a major role in this process. HB-EGF is a single transmembrane-spanning protein that is proteolytically cleaved at a juxtamembrane site, leading to the shedding of soluble EGFR ligand, which in turn activates the EGFR in an autocrine/paracrine manner (17).

The physiological functions as well as the underlying cellular and molecular mechanisms of AT1R in the cardiovascular system have been the focus of many studies, whereas the role of Ang II receptors in skin is not well established. It has been reported that adult rat skin contains predominantly AT1R (18) and that Ang II accelerates the closure of thermal injuries and full-thickness dermal lesions. Both of these responses are associated with the enhancement of several physiological processes necessary for skin wound repair, such as the proliferation of keratinocytes and the production of extracellular matrix (19–21).

As AT1R is a GPCR and as HB-EGF plays an important role in skin wound healing, we investigated the involvement of Ang II-AT1R in skin wound healing. Our results clearly demonstrated that Ang II participates in skin wound healing by accelerating both keratinocyte and fibroblast migration in a process mediated by HB-EGF shedding.

EXPERIMENTAL PROCEDURES

Cell Culture and Reagents—Normal human epidermal keratinocytes were cultured in MCDB 153 type II medium as described previously (22). Keratinocytes in their fourth passage were used in this study. Nor-

* This work was supported in part by a grant for scientific research from the Ministry of Education, Culture, Sports, Science, and Technology of Japan and by a grant for Research on Specific Disease from the Ministry of Health, Labor, and Welfare of Japan. The costs of publication of this article were defrayed in part by the payment of page charges. This article must therefore be hereby marked "*advertisement*" in accordance with 18 U.S.C. Section 1734 solely to indicate this fact.

[1] These authors contributed equally to this work.
[2] To whom correspondence should be addressed. Tel.: 81-89-960-5350; Fax: 81-89-960-5352; E-mail: shirakat@m.ehime-u.ac.jp.

[3] The abbreviations used are: Ang II, angiotensin II; AT1R, angiotensin II type 1 receptor; AT2R, angiotensin II type 2 receptor; TGF-β, transforming growth factor-β; PDGF, platelet-derived growth factor; EGF, epidermal growth factor; EGFR, epidermal growth factor receptor; HB-EGF, heparin-binding EGF like growth factor; GPCR, G protein-coupled receptor; DMEM, Dulbecco's modified Eagle's medium; FCS, fetal calf serum; RT, reverse transcription; MMP, matrix metalloproteinase.

TABLE 1
RT-PCR primers used in this study

hAT1R, upper; 5′-GGC CAG TGT TTT TCT TTT GAA TTT AGC AC
hAT1R, lower: 5′-TGA ACA ATA GCC AGG TAT CGA TCA ATG C
hAT2R, upper: 5′-GTT CCC CTT GTT TGG TGT AT
hAT2R, lower: 5′-CAT CTT CAG GAC TTG GTC AC
mAT1R, upper: 5′-GCA TCA TCT TTG TGG TGG G
mAT1R, lower: 5′-GAA GAA AAG CAC AAT CGC C
mAT1aR, upper: 5′-GCA TCA TCT TTG TGG TGG G
mAT1aR, lower: 5′-ATC AGC ACA TCC AGG AAT G
mAT1bR, upper: 5′-GCATCATCTTTGTGG TGGG
mAT1bR, lower: 5′-ATG AGC ACA TCC AGA AAA C
mAT2R, upper: 5′-AGT GCA TGC GGG AGC TG
mAT2R, lower: 5′-GAC AAC AAA ACA GTG AG

mal human dermal fibroblasts were isolated from normal human skin and cultured in Dulbecco's modified Eagle's medium (DMEM; Invitrogen) supplemented with 10% fetal calf serum (FCS). Fourth- or fifth-passage cells were used. Mouse dermal fibroblasts were isolated from neonatal wild-type and AT1aR−/− mice and cultured in DMEM/10% FCS. Fourth-passage cells were used. Recombinant Ang II, PD123319, and CRM197 were purchased from Sigma. Valsartan, an AT1 receptor-selective blocker, was provided by Novartis Pharma AG (Basel, Switzerland). Anti-HB-EGF neutralizing antibody was purchased from R&D Systems (Tokyo, Japan). GM6001 and AG1478 were purchased from Calbiochem.

RT-PCR—Total RNA was extracted from cultured keratinocytes and fibroblasts using ISOGEN (Nippon Gene, Tokyo, Japan). Human AT1R and AT2R mRNAs and mouse AT1aR, AT1bR, and AT2R mRNAs were analyzed by RT-PCR using the primers listed in Table 1. RT-PCR was performed using RT-PCR High Plus (Toyobo Co., Ltd, Osaka, Japan) according to the manufacturer's instructions. The cDNA was reverse-transcribed from total RNA for 30 min at 60 °C and was heated to 94 °C for 2 min. The amplification was performed using a DNA thermal cycler (Astec, Fukuoka, Japan) for 25 cycles of denaturation for 1 min at 94 °C and annealing and primer extension for 1.5 min at 60 °C.

Migration Assay—Migration was evaluated using a modified Boyden chamber assay, as described previously (23). Briefly, a Nucleopore polyvinylpyrrolidine-free polycarbonate filter (8 μm; Neuro Probe, Inc., Gaithersburg, MD) was coated with type I collagen (Nitta Gelatin, Tokyo, Japan) for 30 min at room temperature and allowed to air dry. The filter was placed over a 48-well chamber containing various concentrations of Ang II in MCDB 153 without bovine pituitary extract for keratinocytes and in DMEM/2% FCS for fibroblasts. After trypsinization, 1×10^4 cells in 50 μl of serum-free MCDB 153 or DMEM were added to the wells in the upper chamber. The chamber was then placed in a humidified incubator at 37 °C for 7 h, after which the upper surface of the filter was scraped to remove non-migratory cells. The filter was subsequently fixed in buffered formalin for 30 min, washed with phosphate-buffered saline, and stained with hematoxylin and eosin. The total number of cells per well was counted by microscopy.

Proliferation Assay—Keratinocytes or fibroblasts were seeded on 6-well plates (5×10^4 cells/well). Next day, medium was replaced to basal medium (MCDB 153 for keratinocytes, DMEM/2% FCS for fibroblasts), and various concentrations of Ang II were added to the medium. After 4 days cell number was counted using Coulter Counter (Z1, Coulter).

Western Blot Analysis—Cells were harvested by scraping with extraction buffer containing 150 mM NaCl, 1% Nonidet P-40, 0.5% deoxycholate, 0.1% SDS, 50 mM Tris-HCl (pH 7.4), and protease inhibitors. Equal amounts of protein were separated by SDS-PAGE and transferred to polyvinylidene difluoride membranes. Primary antibodies (anti-EGFR and anti-phospho-EGFR; Transduction Laboratories, Lexington, KY) were incubated with the membranes at 4 °C overnight. Fluorescein-labeled goat anti-mouse or anti-rabbit IgG (GE Healthcare Biosciences Corp.) was used as the secondary antibody. The signal was amplified with an anti-fluorescein antibody followed by a fluorescent substrate, AttoPhos (GE Healthcare Biosciences Corp.). The membrane was scanned using FluorоImager (GE Healthcare Biosciences Corp.), and each band intensity was quantified with ImageQuant™ (GE Healthcare Biosciences Corp.). The control signal was defined as one unit.

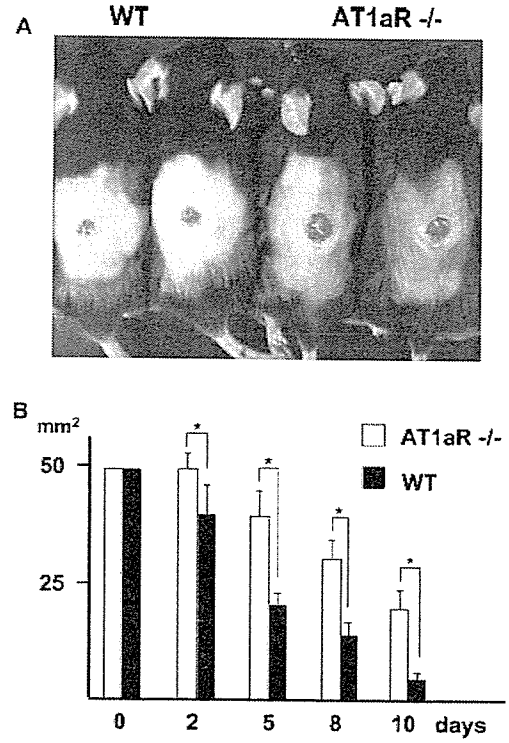

FIGURE 1. **Wound healing assay in AT1aR−/− mice.** An 8-mm punch biopsy was made in the back skin of 8-week-old female wild-type (*WT*) mice and AT1aR−/− mice, and wound closure was monitored. *A*, macroscopic view of wound healing on day 5. *B*, wound area measurement. *, $p < 0.05$.

AT1aR Knock-out Mice—AT1aR knock-out (AT1aR−/−) mice (based on C57BL/6J strain) (24) and wild-type mice were donated by Tanabe Seiyaku Co. Ltd., Osaka, Japan. The Animal Studies Committee of Ehime University approved the following experimental protocol.

Wound Healing Assay—Full-thickness, 8-mm punch biopsy wounds were made on the backs of 8-week-old female C57BL/6 wild-type mice and AT1aR−/− mice ($n = 6$). The edges of the wound were traced onto a clear film immediately after wounding. After treatment, the wounds were covered with a semipermeable polyurethane dressing. Wound areas were measured on days 0, 2, 5, 8, and 10.

Statistical Analysis—The results are representative of three independent experiments. p values were calculated using a two-sided Student's t test (see Figs. 1, 3, 4, 6, and 7; *NS*, not significant; *, $p < 0.05$).

RESULTS

Wound Healing in the AT1aR−/− Mouse—The *in vivo* function of Ang II was investigated in AT1aR knock-out mice. Full-thickness, 8-mm round wounds were prepared on the backs of 8-week-old female C57BL/6 wild-type mice and AT1aR−/− mice. In wild-type mice, the wound areas had decreased to 80% their original size by day 2, but the wound areas were unchanged in AT1aR−/− mice. On day 5, the wound areas were about 50% their original size in wild-type mice but 80% in